

# 1 What caused the interdecadal shift of the ENSO impact 2 on dust mass concentration over northwestern South Asia?

3 Lamei Shi<sup>1,2</sup>, Jiahua Zhang<sup>1,2</sup>, Da Zhang<sup>1,2</sup>, Jingwen Wang<sup>1,2</sup>, Xianglei Meng<sup>2</sup>, Yuqin  
4 Liu<sup>3</sup>, Fengmei Yao<sup>2</sup>

5 <sup>1</sup>Key Laboratory of Digital Earth Science, Aerospace Information Research Institute, Chinese Academy  
6 of Sciences, Beijing 100094, China

7 <sup>2</sup>College of Earth and Planetary Sciences, University of Chinese Academy of Sciences, Beijing 101407,  
8 China

9 <sup>3</sup>Key Laboratory of Urban Environment and Health, Institute of Urban Environment, Chinese Academy  
10 of Sciences, Xiamen 361021, China

11 *Correspondence to:* Jiahua Zhang ([zhangjh@radi.ac.cn](mailto:zhangjh@radi.ac.cn))

12 **Abstract.** The changes of large-scale circulation, especially El Niño-Southern Oscillation (ENSO), have  
13 significant impacts on dust activities over the dust source and downwind regions. However, these impacts  
14 present an interdecadal pattern and it remains less clear that which factors lead to the interdecadal  
15 variability of the ENSO impact on dust activities over the northwestern South Asia, although previous  
16 studies have discussed the response of the interannual dust activities over the northwestern South Asia  
17 to the ENSO cycle. Based on the linear regression model and MERRA-2 atmospheric aerosol reanalysis  
18 data, this study investigated the interdecadal variability of the ENSO impact on dust activities as well as  
19 the associated possible atmospheric drivers under two different warming phases over the northwestern  
20 South Asia. Results indicated that the relationship between ENSO and Dust Column Mass Density  
21 (DUCMASS) experienced an obvious shift from the accelerated global warming period (1982–1996) to  
22 the warming hiatus period (2000–2014). The change of Atlantic and Indian ocean SSTA pattern  
23 weakened the impact of ENSO on dust activities over the northwestern South Asia during 1982–1996,  
24 while the change of PDO strengthened ENSO’s effect when it was in phase with ENSO. Both the Atlantic  
25 and Indian Ocean SSTA patterns were modulated by the duration of ENSO events (i.e., continuing and  
26 emerging ENSO). This study provides new sights to numerical simulation involving the influence of  
27 atmospheric teleconnections on the variability of dust activities and their influence mechanisms.

28 **Keywords:** Surface dust mass concentration; ENSO–DUCMASS relationship; interdecadal change;  
29 large-scale atmospheric circulation; northwestern South Asia

## 30 1 Introduction

31 Dust aerosol is attracting an increasing concern due to its adverse impacts on human health  
32 (Bozlaker et al., 2013; Chen et al., 2004; Erel et al., 2006; Kaiser and Granmar, 2005; Poulsen et al.,  
33 1995; Sanchez de la Campa et al., 2013; Schulz et al., 2012) and environmental problems (Avila, 1998;  
34 Behrooz et al., 2017; Razakov and Kosnazarov, 1996). The Northwest Indian subcontinent, which is the  
35 most arid and semiarid area of South Asia, suffers heavy and frequent dust storms in summer due to  
36 extremely dry climate and strong winds (Jin and Wang, 2018). Those dust can travel long-distance to  
37 North India and the Arabian Sea, degrading air quality (Mahowald et al., 2010) and modifying ocean  
38 biogeochemistry processes (Richon et al., 2018; Singh et al., 2008). Particularly, dust aerosols can change  
39 local radiation budget, circulations, and Indian summer monsoon rainfall through absorption and  
40 scattering of solar radiation. The mineral dust over the northwestern South Asia is closely associated with  
41 the long-term variation of global climate (Banerjee et al., 2019; Bollasina et al., 2011; Jin et al., 2018).  
42 To better understand such feedback, and give early warning to reduce disasters and losses caused by dust  
43 events, it is important to find out the controlling factors of the Dust Column Mass Density (DUCMASS)  
44 and its long-term variation.

45 ENSO, as a periodic fluctuation in sea surface temperature (SST) and the air pressure across the  
46 equatorial Pacific Ocean, is as the primary large-scale driver of dust loading over the global dust source  
47 region (Trenberth et al., 2014). Prospero and Nees (1986) found that ENSO-related large-scale  
48 atmospheric circulation changes led to the increase in winter dust concentration over North Africa. Xi  
49 and Sokolik (2016a) indicated that in La Niña years, the precipitation and soil moisture over Central Asia  
50 decreased and caused poor vegetation conditions and heavy drought conditions, which strengthened dust  
51 activities. Yu et al. (2015b) suggested that La Niña events provided favorable conditions for dust  
52 activities over Saudi Arabia. However, Banerjee et al. (2016) proposed that the low-level southwesterly  
53 winds and high-level westerly winds accompanied with La Niña events were the main factor that  
54 contributed to the elevated dust levels over the Arabia Peninsula. Abish and Mohanakumar (2013)  
55 pointed out that strengthened westerly circulation related with El Niño increased the dust transmission  
56 from the Middle East to the Indian subcontinent. Simultaneously, the impacts of ENSO on dust activities  
57 were also modulated by other atmospheric factors, e.g., PDO could strengthen the effect of ENSO when

58 it was in phase with ENSO (He et al., 2013; Wang et al., 2008; Wang et al., 2014); the spring dust index  
59 over the northern China in the years when negative AO and El Niño occurred synchronously was  
60 significantly higher than that in the years when positive AO and La Niña were concurrent (Liu et al.,  
61 2020; Lee et al., 2015); IOD could also influence the dust activities over the northwestern Indian ocean  
62 by adjusting the El Niño related water vapor conditions (Banerjee and Kumar, 2016).

63 ENSO exhibits profound impacts on the global climate. Nevertheless, the Earth climate is varying  
64 and ENSO, including its feedback and influences on the changing global climate, also experience  
65 significant changes (Ashok et al., 2007; Weare et al., 1976; Weng et al., 2007; Yang and Jiang, 2014; Yu  
66 and Kao, 2007; Yuan and Yang, 2012). In the mid-1970s, an interdecadal climate regime shift was  
67 observed in the large-scale boreal winter circulation pattern over the North Pacific (Graham, 1994; Nitta  
68 and Yamada, 1989; Trenberth and Hurrell, 1994). Another remarkable climate change was observed in  
69 the early 21<sup>st</sup> century, i.e., an accelerated global warming prevailed before late 1990s and a warming  
70 hiatus dominated after that (Easterling and Wehner, 2009; Fyfe et al., 2011, 2013). After 2013, the global  
71 warming hiatus came to an end due to a persistent warm condition over the equatorial Pacific between  
72 Mar. 2014 and May 2016 (Hu and Fedorov, 2017). Concurrent with the Pacific climate shift, the large-  
73 scale circulation pattern and their atmospheric teleconnection also exhibited an interdecadal change, e.g.,  
74 the correlation between El Niño and rainfall over India turned to be insignificant from the late 1970s,  
75 simultaneously, the relationship between ENSO and monsoon also weakened around this turning point  
76 (Kumar et al., 1999). Two influence mechanisms were proposed to explain this weakened ENSO–  
77 monsoon relationship. One was the varied location of Walker circulation that adjusted the monsoon  
78 rainfall over Indian region, the other was the temperature change over Eurasia that modulated the land-  
79 sea thermal gradient. Besides, the impact of Atlantic Ocean pattern on the monsoon circulation over the  
80 Indian Ocean became stronger since late 1970s as the influence of the tropical Pacific has reduced  
81 (Kucharski et al., 2007; Sabeerali et al., 2019; Srivastava et al., 2019). This in-turn impacted the  
82 circulation responsible for dust uplift and transport.

83 It was reported that the effect of ENSO on Indian summer monsoon rainfall (ISMR), which was an  
84 important modulator to DUCMASS, experienced a remarkable interdecadal change and many factors  
85 may cause this transition (Yang and Huang, 2021). Till now, the interdecadal variability in the links of

86 DUCMASS over the northwestern South Asia with ENSO has not been fully investigated, as compared  
87 to the North African and West Asian counterpart (Yu et al., 2015). In addition, though many factors have  
88 been proved to influence the short-term (e.g., interannual scale) variation of the relationship between  
89 ENSO and dust activities over South Asia, their effects on the long-term (e.g., interdecadal scale) change  
90 are still unclear. Cai et al. (2014) pointed out that global warming will have a significant impact on ENSO.  
91 The extreme El Niño events will become more frequent under the changes of atmospheric convection in  
92 the next half of the 21<sup>st</sup> century. Thus, understanding the physical mechanism of the shifting ENSO–  
93 DUCMASS relationship is of profound implications for the forecast of dust trend in the future climate  
94 change scenario. This study aims to investigate the large-scale atmospheric factors that contribute to the  
95 interdecadal variability of the ENSO impact on DUCMASS over the northwestern South Asia.

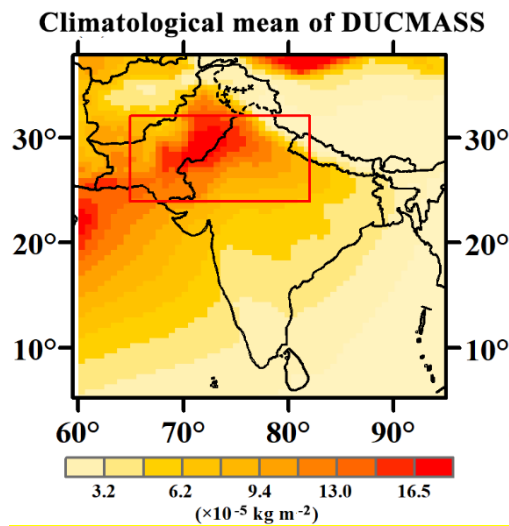
96 The paper is organized in the following structure: section 2 describes the datasets and methods;  
97 section 3 presents factors that influence the interdecadal change of the relationship between DUCMASS  
98 and wintertime Niño-3 index; section 4 discusses the deficiency and prospect of this study, and the  
99 conclusions are given in section 5.

## 100 **2 Data and methods**

### 101 **2.1 Study area**

102 The main dust source over South Asia is a large arid region in the northwestern part of the Indian  
103 subcontinent, which stretches from India to Pakistan. Most of the dust aerosols over this region come  
104 from the Thar desert. The southeastern part of the Thar desert lies between the Aravalli Hills. The desert  
105 extends as far as the Punjab Plain in the north and northeast, the alluvial plains of the Indus River in the  
106 west and northwest, and the Great Rann of Kutch along the western coast. The desert presents an  
107 undulating surface, with high and low sand dunes separated by sandy plains and low barren hills. The  
108 soils are mainly consisted by desert soils, red desertic soils, sierozems, the red and yellow soils of the  
109 foothills, the saline soils of the depressions, and the lithosols (shallow weathered soils) and regosols (soft  
110 loose soils) found in the hills. The subtropical desert climate here results from persistent high pressure  
111 and subsidence. The prevailing southwest monsoon winds from Indian Ocean that bring rain to much of  
112 the Indian subcontinent in summer tend to bypass the Thar to the east. The soils are generally infertile

113 and overblown with sand due to severe wind erosion (Augustyn et al., 2019). The amount of annual  
114 rainfall in the desert is low, ranging from about 100 mm or less in the west to about 500 mm in the east.  
115 Almost 90 % of the annual rainfall occurs in the season southwest monsoon, from July to September.  
116 While the prevailing wind is dry northeast monsoon during other seasons. Dust storms and dust-raising  
117 winds are common from May to July (Chauhan, 2003). Thus, the DUCMASS used in this study is  
118 averaged from June to July and May is neglected to eliminate the disturbance of seasonal climatological  
119 differences. Analysis is carried out over the dust source in the northwestern South Asia ( $65^{\circ}$ – $82^{\circ}$  E,  $24^{\circ}$ –  
120  $32^{\circ}$  N), as shown in Fig. 1. All variables involving spatial average are taken from this region unless stated  
121 otherwise.



122  
123 **Figure 1: Climatological mean DUCMASS over South Asia based on the MERRA-2 dataset. The dust source**  
124 **over the northwestern South Asia is marked with red rectangle.**

## 125 2.2 Datasets

### 126 2.2.1 Dust concentration

127 Dust column mass density from 1982 to 2014 was obtained from the Modern-Era Retrospective  
128 Analysis for Research and Applications, version 2 (MERRA-2). MERRA-2 is produced via the Goddard  
129 Earth Observing System-Data Assimilation System (GEOS-DAS, version 5.12.4) based on GEOS-5  
130 climate model and the Gridpoint Statistical Interpolation (GSI) analysis scheme (Gelaro et al., 2017).  
131 Extensive satellite data are integrated into MERRA-2 to estimate dust concentration (Randles et al., 2017;  
132 Veselovskii et al., 2018). The dust products were comprehensively validated using the results of ground-  
133 based observation, satellite measurements, and numerical simulation (Buchard et al., 2017; Randles et

134 al., 2017). They have been widely applied to researches on global environment and climate change (He  
 135 et al., 2019; Randles et al., 2017). The variable “Dust Column Mass Density-PM<sub>2.5</sub>” (DUCMASS25)  
 136 with a spatial resolution of 0.625°×0.5° (longitude×latitude) used in this study is from the dataset of  
 137 “tavGM\_2d\_aer\_Nx”.

### 138 2.2.2 Land and sea surface temperature

139 To explore the possible influence of SST on the South Asian dust activity, we used three SST  
 140 datasets from 1981 to 2014 for comparison: (1) The National Oceanic and Atmospheric Administration  
 141 (NOAA) Extended Reconstructed SST (ERSST) version 5 (Huang et al., 2017) that is available at 2°×2°  
 142 spatial resolution is used for analysis, (2) Centennial in situ Observation-Based Estimates (COBE)  
 143 version 2 SST data at 1°×1° spatial resolution (Hirahara et al., 2014) and (3) Hadley Centre Global Sea  
 144 Ice and Sea Surface Temperature (HadISST1.1) dataset produced by the Met Office, starting from 1870  
 145 up to the present with a horizontal resolution of 1°×1° (Rayner et al., 2003). While the land-sea thermal  
 146 contrast was calculated from the Hadley Centre Climate Research Unit Temperature version 5.0.1.0  
 147 (HadCRUT5) data from 1981 to 2014, which is a blend of the Climatic Research Unit land-surface air  
 148 temperature dataset (CRUTEM5) and the Hadley Centre sea-surface temperature (HadSST4) dataset  
 149 (Osborn et al., 2021). The longitude and latitude of SST index involved in this study were shown in Table  
 150 1.

151 **Table 1: Longitude and latitude of SST index used in this study.**

Acronyms	Full Name	Longitude and Latitude	Involved Ocean
Niño-3	—	150°–90° W, 5° S–5° N	Pacific
Niño-3.4	—	170°–120° W, 5° S–5° N	Pacific
Niño-4	—	160° E–150° W, 5° S–5° N	Pacific
ASGI	Atlantic SSTA gradient index	North: 60°–30° W, 0–20° N South: 20° W–10° E, 0–20° S	Atlantic Ocean
TWISSTA	Tropical western Indian ocean SSTA	50°–70° E, 10° S–15° N	Indian Ocean
<b>IOD</b>	<b>Indian Ocean Dipole</b>	<b>West: 50°–70° E, 10° S–10° N</b> <b>East: 90°–110° E, 10° S–0°</b>	<b>Indian Ocean</b>

152 **2.2.3 Large-scale climate indices**

153 Three monthly Niño indices Niño-3, Niño-3.4, and Niño-4 from 1981 to 2014, which monitor the  
154 SST anomalies averaged across the eastern equatorial Pacific, Pacific from dateline to the South  
155 American coast, and central equatorial Pacific, respectively, were used to analyze their links with  
156 DUCMASS over the northwestern South Asia. Kinter et al. (2002) pointed out that Nov.–Jan. is the peak  
157 season for El Niño/La Niña, thus the average Niño index from (–1) Nov. to (0) Jan. was used. Only one  
158 Niño index that showed the highest correlation coefficient was retained in this study, i.e., Niño-3. The  
159 time series of ENSO was represented by Niño-3 and Niño-3 also referred to ENSO. The large-scale  
160 climate indices, such as PDO and IOD, was also used to explore the potential factors that contributed to  
161 the interdecadal shift of ENSO–DUCMASS relationship. All those indices were from the Climate Predict  
162 Center of National Oceanic and Atmospheric Administration (NOAA/CPC).

163 **2.3 Method**

164 In this study, we compared the impact of ENSO on DUCMASS over the northwestern South Asia  
165 under two different warming epochs, and investigated the potential global change drivers to the shift of  
166 ENSO–DUCMASS relationship. The global warming was separated into the accelerated warming period  
167 from 1982 to 1996 (P1) and the warming hiatus period from 2000 to 2014 (P2). The year 2014 was added  
168 to the warming hiatus period to keep the length of those two periods consistent. This classification was  
169 not controversial since the ENSO year stated in this study spanned from antecedent November to current  
170 January.

171 **2.3.1 Contribution of factors to relationship**

172 The contribution of X (Indian Ocean SSTA, Atlantic SSTA gradient index, and PDO) modifying  
173 ENSO–DUCMASS relationship was defined as: sliding regression of X onto Niño-3 index multiplies by  
174 sliding regression of DUCMASS onto X with Niño-3 removed (Yang and Huang, 2021).

175 **2.3.2 Signal removal method**

176 The ENSO signals were removed from the oceanic SSTA pattern when analyzing spatial coupling

177 and regression mode between the oceanic SSTA pattern and DUCMASS as well as local surface  
178 conditions (precipitation, soil moisture, land cover, wind, etc). Simultaneously, the oceanic SSTA signals  
179 were removed from ENSO when calculating the sliding correlation between ENSO and DUCMASS. In  
180 this study, the residual time series based on the linear regression method were used to represent the ENSO  
181 (or oceanic SSTA index)-independent components (Yang and Huang, 2021), as shown in Eq. (1):

$$\xi_{remove} = \xi - Z \times \frac{cov(\xi, Z)}{var(Z)} \quad (1)$$

182 Where  $\xi_{remove}$  is the time series of variable  $\xi$  with  $Z$  removed,  $\xi$  is the time series of original  
183 variable,  $Z$  is the time series of related signal that needs to be removed,  $cov$  indicates the covariance  
184 between two variables, and  $var$  indicates the variance of ENSO.

### 185 2.3.3 Coupled spatial pattern analysis

186 The maximum covariance analysis (MCA) is a useful tool for isolating the most coherent pairs of  
187 spatial patterns and their associated time series by performing an eigenanalysis on the temporal  
188 covariance matrix between two geophysical fields (Storch and Zwiers, 1999). The MCA method was  
189 used to analyze the coupled patterns between DUCMASS and oceanic SSTA.

### 190 2.3.4 Definition of different types of ENSO

191 Following Yang and Huang (2021), the EM and CT ENSO were defined based on the three-month  
192 running mean of the Niño-3 index. Two situations for the CT ENSO were considered, i.e., the slowly  
193 decaying events and the developing events since the previous winter. For the slowly decaying situation,  
194 a CT ENSO was identified when the average Niño-3 of (−1) Oct.–(0) Jan. was greater than 0.5 (below −  
195 0.5) standard deviation (STD), became greater than 0.5 (below −0.5) STD in single month during (0)  
196 Mar.–(0) May, and remained positive (negative) during (0) Jun.–(0) Sep.. For the developing events since  
197 the previous winter, a CT ENSO was identified when the Niño-3 was greater than 0.75 (below −0.75)  
198 STD in any month from (−1) Oct. to (0) May, accompanied by positive (negative) values for eight single  
199 months, and the average Niño-3 of (0) Jun.–(0) Sep. was greater than 0.5 (below −0.5) STD. To acquire  
200 more available samples in the study period, all the ENSO years that were not defined as CT ENSO were  
201 identified as EM ENSO year in this study, which was different from Yang and Huang (2021). Based on  
202 this definition, the CT El Niño years during 1982–2014 included 1982, 1983 and 1987; CT La Niña years



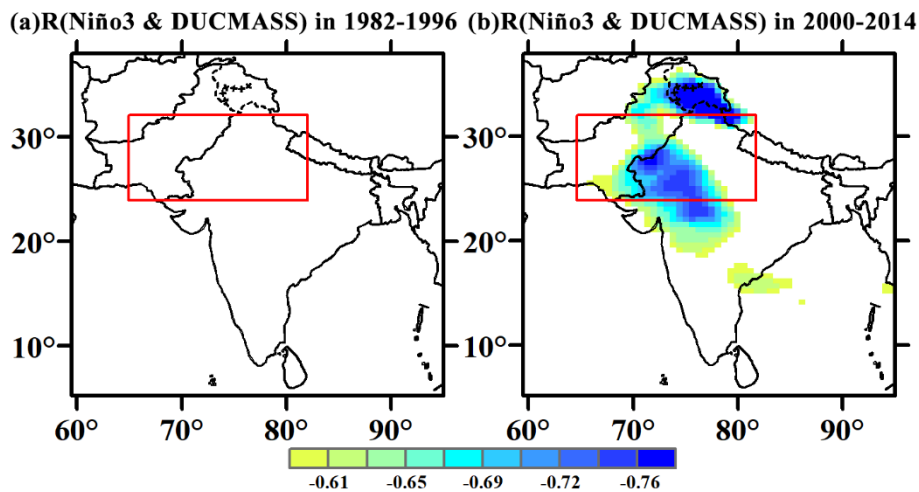
203 included 1984, 1985, 1989, 1996, 1999, 2000, and 2011; EM El Niño years included 1995, 1998, 2003,  
204 2005, 2007, and 2010; EM La Niña years included 2008 and 2012.

205 In this study, “(0) month” represented the year concurrent with the year when DUCMASS was  
206 acquired and “(-1) month” represented the preceding year.

## 207 3 Results

### 208 3.1 Observed interdecadal change of the impact of ENSO on DUCMASS

209 In the present study, we found that the DUCMASS–Niño-3 relationship experienced an interdecadal  
210 transition at around 1999/2000. Based on the 15-year sliding correlation from 1982 to 2014 (Fig. 4 (a)),  
211 the DUCMASS–Niño-3 relationship was weak before the early of 2000s and became stronger after that.  
212 Specifically, the winter Niño-3 index ((-1) Nov.–(0) Jan.) presented a significant negative relation ( $R=-$   
213  $0.68$ ,  $p<0.01$ ) with DUCMASS during 2000–2014 (P2), while no significant correlation ( $R=-0.41$ ,  
214  $p>0.05$ ) was observed in 1982–1996 (P1), as shown in Fig. 2.



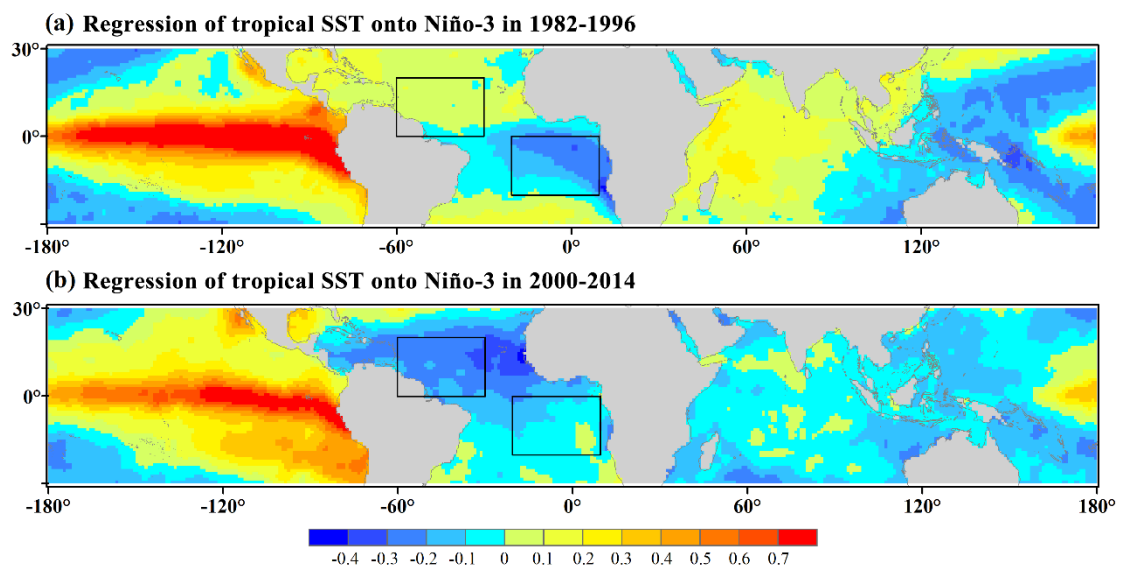
215  
216 **Figure 2: Correlation between Niño-3 index and DUCMASS over South Asia during (a) 1982–1996 and (b)**  
217 **2000–2014. (Only correlations that passed the 99% confidence level were presented).**

### 218 3.2 Factors influencing the interdecadal change of the impact of ENSO on DUCMASS

#### 219 3.2.1 Tropical Atlantic SSTA pattern

220 With the global climate change observed in early 2000s, the ENSO-related tropical Atlantic SSTA  
221 experienced an obvious transition, i.e., from an Atlantic Niña pattern during 1982–1996 to an Atlantic  
222 Niño pattern during 2000–2014 (Fig. 3), which coincides with the findings of Yang and Huang (2021).

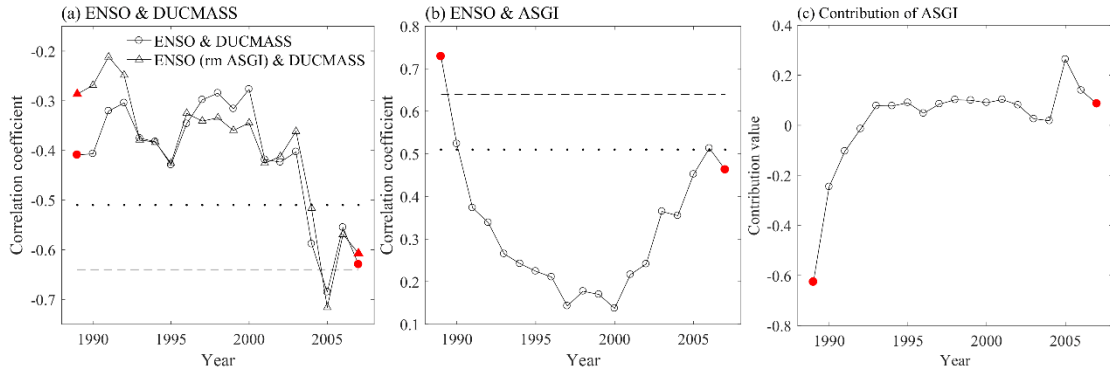
223 The tropical Atlantic SSTA pattern was a crucial factor for the restoration of ENSO–ISMR relationship  
 224 since the late 1990s (Yang and Huang, 2021), thus, it could also disturb the impact of ENSO on dust  
 225 activities over the northwestern South Asia. In order to validate the connection between the Atlantic  
 226 SSTA and the DUCMASS–Niño-3 relationship, an Atlantic SSTA gradient index (ASGI) was used to  
 227 describe the SSTA pattern shift in the tropical Atlantic, which represented the difference of averaged  
 228 SSTA between tropical North Atlantic and tropical South Atlantic (marked by two rectangles in Fig. 3).  
 229 According to Tokinaga et al. (2019), the Atlantic Niña pattern develops and is most sensitive to ENSO  
 230 in spring, thus the SST averaged from Mar. to May was used in this section.



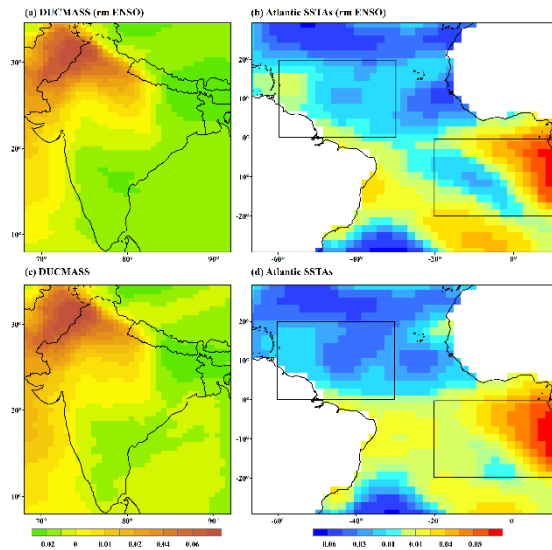
231  
 232 **Figure 3: Regression of spring (Mar.–May) tropical SSTA onto Niño-3 index. Black rectangles denote the**  
 233 **regions to define ASGI. The range of the upper one is 60–30° W, 0–20° N and that of the lower one is 20° W–**  
 234 **10° E, 20–0° S. (Similar with Fig. 2 (c)–(d) of Yang and Huang (2021) but with different time spans)**

235 The relationship between Niño-3 and DUCMASS witnessed a reversal at the early 2000s,  
 236 simultaneously, the correlation between Niño-3 and ASGI exhibited the similar change. The correlation  
 237 between Niño-3 and ASGI passed the 99% confidence level during P1, while it did not pass the 95%  
 238 confidence level during P2, as shown in Fig. 4 (b). However, the correlation between Niño-3 and  
 239 DUCMASS showed a contrary trend with a higher correlation coefficient appeared in P2. Figure 4 (a)  
 240 showed that the DUCMASS–Niño-3 relationship was weakened when the ASGI signals were removed  
 241 from Niño-3 index during P1, while during P2, the DUCMASS–Niño-3 relationship remained the same  
 242 with or without the ASGI signals removed. In addition, the contribution of ASGI to the DUCMASS–  
 243 Niño-3 relationship (Fig. 4 (c)) proved that during P1, ASGI weakened this relationship while no

244 significant contribution was observed during P2. Thus, it is hypothesized that the strengthening  
 245 (weakening) of the response of ASGI to Niño-3 weakened (strengthened) the impact of Niño-3 on  
 246 DUCMASS during P1 (P2).



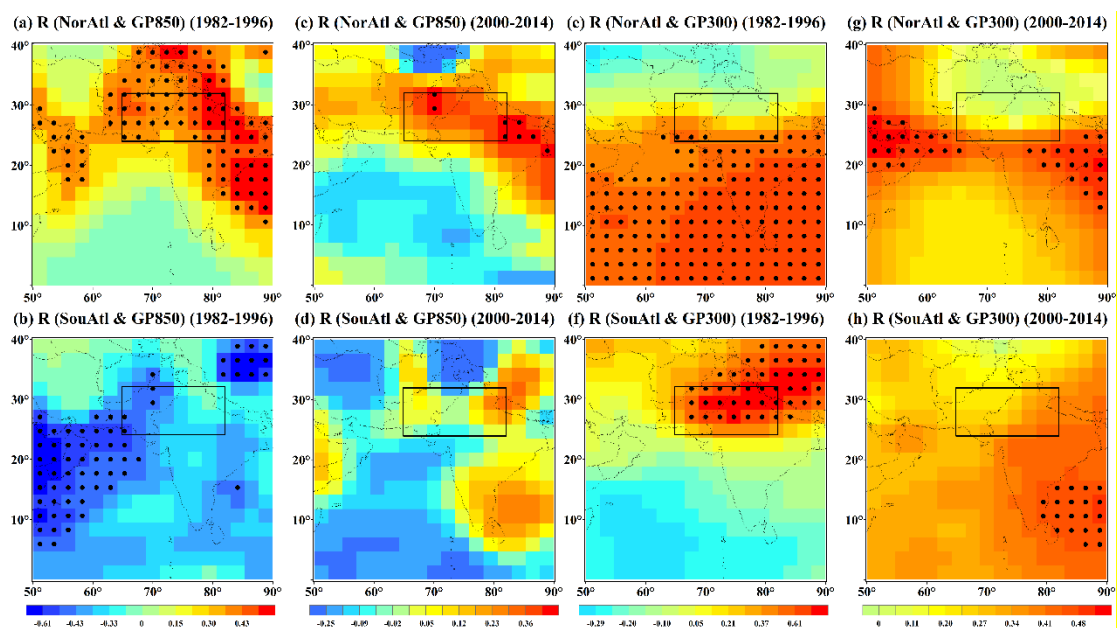
247  
 248 **Figure 4: (a) The 15-year sliding correlation between DUCMASS and Niño-3 with and without ASGI-related**  
 249 **signals removed; (b) 15-year sliding correlation between Niño-3 and ASGI; (c) Sliding contribution of ASGI**  
 250 **to DUCMASS–Niño-3 relationship. The two red filled markers represented the 15-year window spanning**  
 251 **from 1982 to 1996 and 2000 to 2014, respectively. The x-axis denotes the middle year of the period under**  
 252 **analysis.**



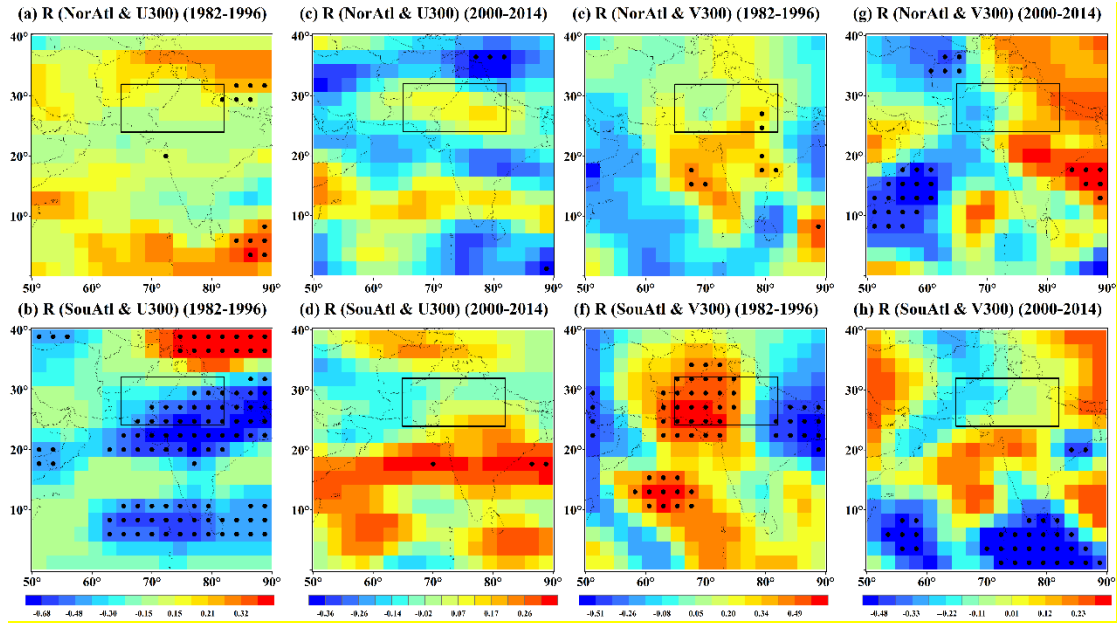
253  
 254 **Figure 5: Spatial correlation between spring (Mar.–May) tropical Atlantic SSTA and DUCMASS of the first**  
 255 **mode of the MCA analysis in 1982–2014. The first MCA mode of (a) the DUCMASS, and (b) the tropical**  
 256 **Atlantic SSTA with ENSO-related signals removed. (c)–(d) As in (a)–(b), but for the original series including**  
 257 **the ENSO signal.**

258 In order to validate the effect of Atlantic SSTA pattern on the DUCMASS–Niño-3 relationship, the  
 259 spatial coupling mode between DUCMASS and tropical Atlantic SSTA was explored. Figure 5 showed  
 260 that the negative ASGI, i.e., negative SST anomaly over the tropical North Atlantic and positive SST  
 261 anomaly over the tropical South Atlantic, was coupled with increased DUCMASS over the northern and

262 northwestern India. This pattern was not impacted by ENSO since the MCA results with ENSO-related  
 263 signals removed were similar with that including the ENSO-related signals, as shown in Fig. 5. Figures  
 264 6 and 7 further illustrated the influence mechanism of Atlantic SSTA pattern onto DUCMASS. Figure 6  
 265 showed that the effect of North and South Atlantic SSTA (NorAtl/SouAtl) with ENSO signal removed  
 266 on the geopotential height (GP) at 850hPa/300hPa exhibited significant difference during P1, while they  
 267 were close (all are not significant) in P2. Similarly, significant difference was also seen in the effect of  
 268 North and South Atlantic SSTA on the zonal/meridional wind (U/V) at 300hPa in P1, which disappeared  
 269 in P2, as shown in Fig. 7. This was consistent with the variation of Atlantic SSTA's contribution to  
 270 DUCMASS–Niño-3 relationship, i.e., during P1, the Atlantic SSTA pattern was featured with a Niña type  
 271 (Fig. 3 (a)), thus the South Atlantic presented stronger influence on the atmospheric circulation over  
 272 South Asia, which weakened the impact of ENSO on DUCMASS; while in P2, the negative North  
 273 Atlantic SSTA (Fig. 3 (b)) decreased the SSTA gradient between North and South Atlantic and offset the  
 274 effect of the Niña pattern, which weakened the response of atmospheric circulation on North and South  
 275 Atlantic SSTA gradient and strengthened the DUCMASS–Niño-3 relationship.



276  
 277 **Figure 6: Correlation between spring (Mar.–May) tropical North and South Atlantic SSTA (NorAtl/SouAtl)**  
 278 **with ENSO signal removed and geopotential height (GP) at 850hPa (a)–(d) as well as 300hPa (e)–(h) in dust**  
 279 **season (Jun.–Jul.). (Correlations that passed the 90% confidence level were marked by black dots).**

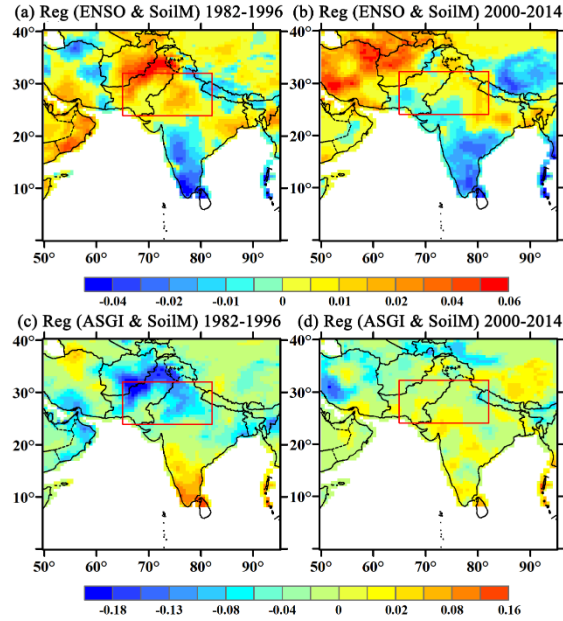


280

281 **Figure 7: Correlation between spring (Mar.–May) tropical North and South Atlantic SSTA (NorAtl/SouAtl)**  
 282 **with ENSO signal removed and zonal wind (U) (a)–(d) as well as meridional wind (V) (e)–(h) at 300hPa in**  
 283 **dust season (Jun.–Jul.). (Correlations that passed the 90% confidence level were marked by black dots).**

284

285 In order to verify the inhibitory effect of Atlantic SSTA pattern on the DUCMASS–Niño-3  
 286 relationship, we analyzed the regression of ASGI onto the local conditions that directly influenced  
 287 DUCMASS, such as precipitation (PPT), soil moisture (Soilm), Normalized Difference Vegetation Index  
 288 (NDVI), and air flow. Figure 8 showed that the regression coefficients between ASGI and Soilm as well  
 289 as PPT and NDVI (not shown) were opposite to that between Niño-3 and Soilm during P1, while during  
 290 P2, the abovementioned differences were weakened. Besides, Figure 9 demonstrated that the regression  
 291 coefficients between Niño-3 and velocity potential (VP) as well as wind field at 200hpa and 850hPa were  
 292 also contrary to the regression coefficients between ASGI and those factors, indicating the opposite effect  
 293 of ASGI and ENSO on local wind field and convection. All of those proved the inhibitory effect of  
 Atlantic SSTA pattern on the DUCMASS–Niño-3 relationship during P1.

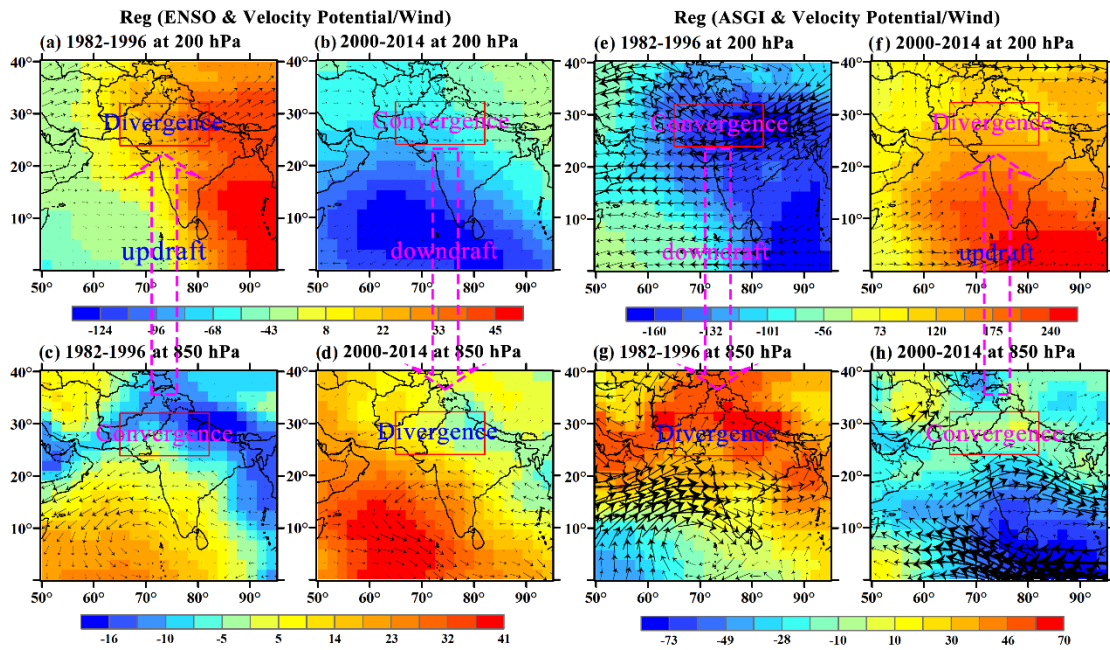


294

295

296

**Figure 8: (a)–(b) Regression of ENSO with ASGI-related signals removed onto SoilM in dust season (Jun.–Jul.); (c)–(d) Regression of ASGI with ENSO-related signals removed onto SoilM in dust season (Jun.–Jul.).**



297

298

299

300

**Figure 9: (a)–(d) Regression of ENSO with ASGI-related signals removed onto velocity potential (VP) and wind at 200hPa and 850hPa in dust season (Jun.–Jul.); (e)–(h) Regression of ASGI with ENSO-related signals removed onto velocity potential and wind at 200hPa and 850hPa in dust season (Jun.–Jul.).**

301

### 3.2.2 Tropical Indian ocean SSTA pattern

302

This study explored the effect of Indian ocean SSTA pattern on the DUCMASS–Niño-3 relationship.

303

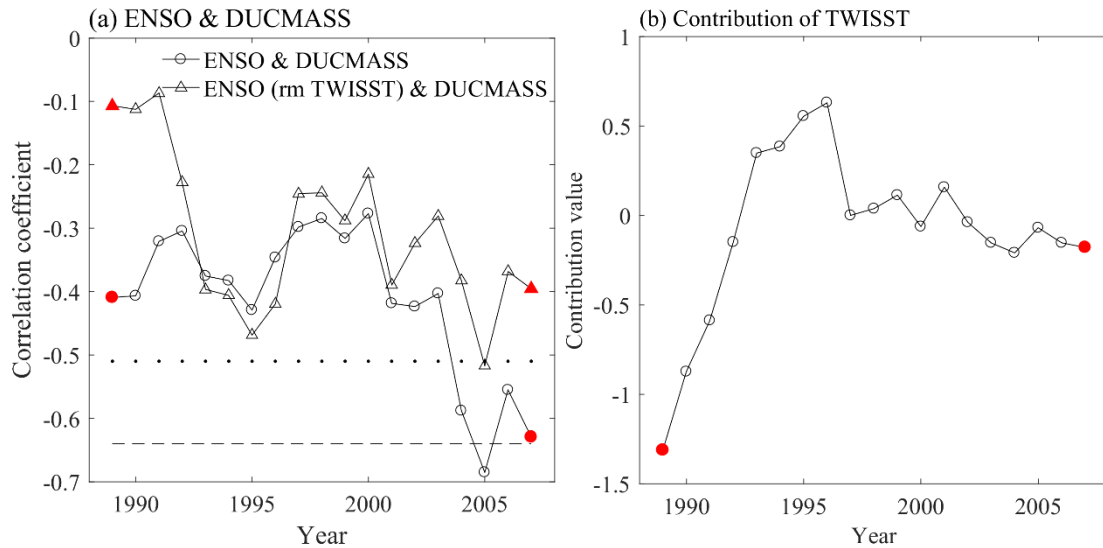
The covariability between the western Pacific and Indian Ocean has been widely recognized by previous

304

studies (Kug et al., 2005; Wang et al., 2003; Watanabe and Jin, 2002). ENSO can affect the Indian Ocean

305 SST in the form of Walker circulation and the Indian Ocean variability can also modulate the ENSO  
306 variability (Kug et al., 2005; Wu and Kirtman, 2004; Yu et al., 2002). It is known that ENSO mainly  
307 influences the monsoon rainfall of South Asia through changing the SST of Indian ocean (Krishnamurthy  
308 and Kirtman, 2003; Srivastava et al., 2019). Du et al. (2009) indicated that the North Indian Ocean  
309 warming displayed two peaks in Nov.–Dec.(–1) and Jun.–Aug.(0), with the second peak larger in  
310 magnitude. Cherchi and Navarra (2013) also pointed out that the connection between ISM and Indian  
311 ocean SST pattern was mostly confined in summer and autumn. Besides, compared to Atlantic, the Indian  
312 ocean is closer to the South Asian dust source, thus it takes less time to transmit the signal (partially  
313 through wave train propagation) from the Indian ocean to the dust source than that from the Atlantic.  
314 Given all of that, the Indian ocean SST used in this study was the summer average that was concurrent  
315 with the dust season (Jun.–Jul.).

316 The relationship between DUCMASS and Niño-3 with Indian ocean SST signal removed also  
317 experienced decadal variation. Figure 10 (a) showed that the correlation between Niño-3 and DUCMASS  
318 was obviously reduced when the tropical western Indian ocean SSTA (TWISST) was removed from  
319 Niño-3. As illustrated by Fig. 10 (b), during P1, TWISST weakened this correlation while no significant  
320 contribution was observed during P2. Thus, it is hypothesized that TWISST weakened the impact of  
321 ENSO on DUCMASS during P1. However, when the IOD (rather than TWISST) was considered, the  
322 correlation between Niño-3 and DUCMASS kept the same when IOD was removed from Niño-3,  
323 indicating that IOD exhibited no significant impact on the correlation between Niño-3 and DUCMASS.  
324 Clark et al. (2000) showed that the SST in the central Indian Ocean exhibited stronger correlation with  
325 the Indian precipitation than that in the Arabian Sea and northwest of Australia. Cherchi and Navarra  
326 (2013) also pointed out that when the eastern and western poles of the IOD were considered separately,  
327 the western side exhibited the largest correlation. Thus, the TWISST was considered when exploring the  
328 effect of Indian ocean SSTA pattern on the DUCMASS–Niño-3 relationship.



329

330 **Figure 10: (a) The 15-year sliding correlation between DUCMASS and Niño-3 with and without TWISST-**  
 331 **related signals removed; (b) Sliding contribution of TWISST to DUCMASS–Niño-3 relationship. The two red**  
 332 **filled markers represented the 15-year window spanning from 1982 to 1996 and 2000 to 2014, respectively.**  
 333 **The x-axis denotes the middle year of the period under analysis.**

334

335

336

337

338

339

340

341

342

343

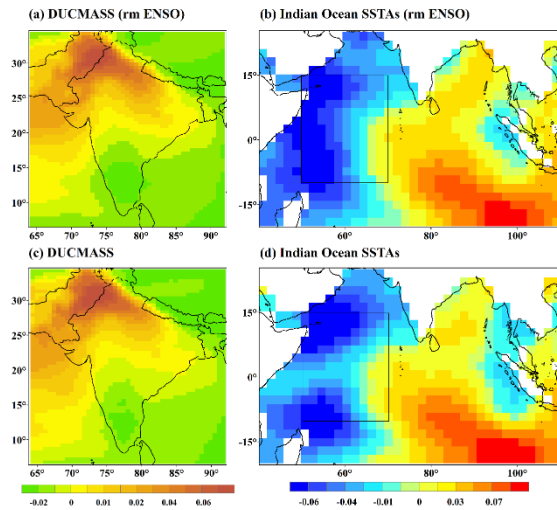
344

345

346

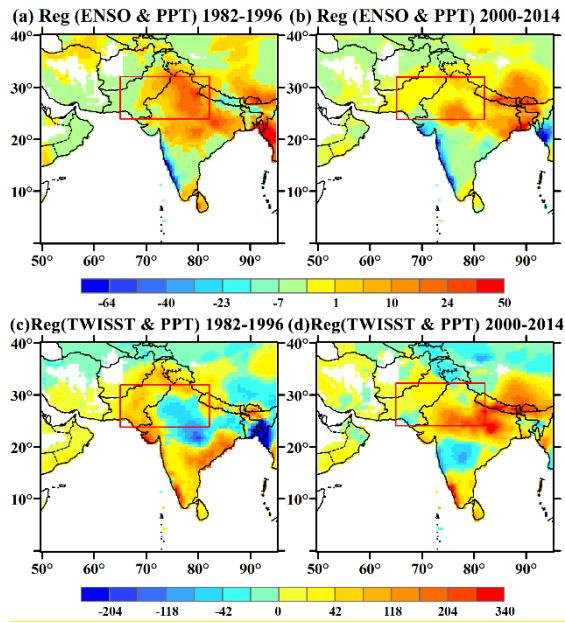
The spatial coupling mode between DUCMASS and tropical Indian ocean SSTA showed that the cold tropical western Indian ocean and warm tropical eastern Indian ocean were coupled with higher DUCMASS over the northern and northwestern India. This pattern was not impacted by ENSO since the MCA results with ENSO-related signals removed were similar with that including the ENSO-related signals, as shown in Fig. 11. Figures 12–14 further illustrated the influence mechanism of Indian ocean SSTA pattern onto DUCMASS. Figure 12 showed that during P1, the regression coefficients between ENSO and PPT were opposite to the that between TWISST and PPT, while during P2, the regression coefficient between ENSO and DUCMASS as well as that between TWISST and DUCMASS were all positive. The similar changes were also seen when the effects of ENSO/TWISST on SoilM (Fig. 13), VP and wind field (Fig. 14) were considered. These illustrated the opposite effect of TWISST and ENSO on the key factors that influence the dust concentration, i.e., the local wind field and surface conditions. The above results further verified the inhibitory effect of Indian ocean SST pattern on the DUCMASS–Niño-3 relationship during P1, as well as the promotional effect during P2.





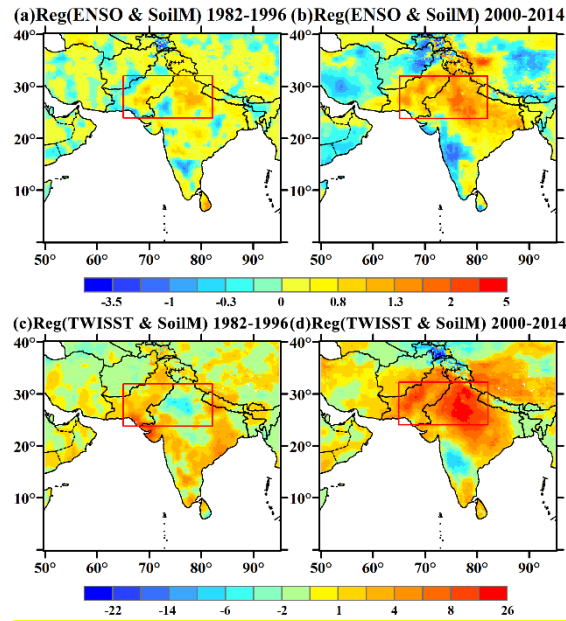
347  
348  
349  
350  
351

**Figure 11: Spatial correlation between summer (Jun.-Jul.) tropical Indian ocean SSTA (TWISSTA) and DUCMASS of the first mode of the MCA analysis in 1982–2014. The first MCA mode of (a) the DUCMASS, and (b) the summer (Jun.-Jul.) tropical Indian ocean SSTA with ENSO-related signals removed. (c)–(d) As in (a)–(b), but for the original series including the ENSO signal.**



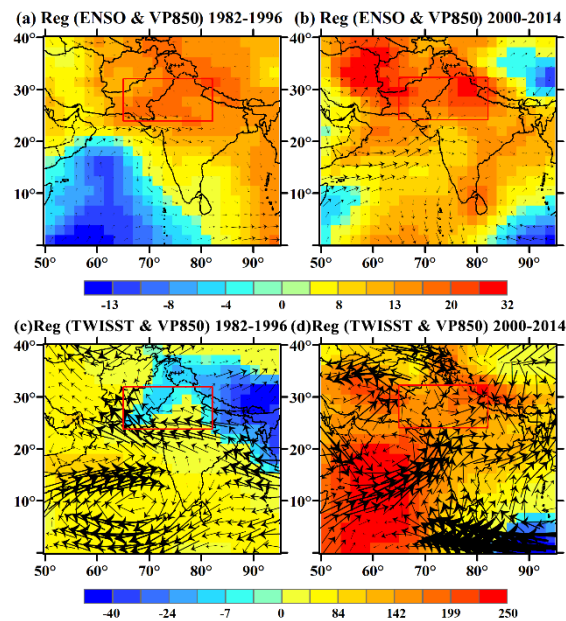
352  
353  
354

**Figure 12: (a)–(b) Regression of ENSO with TWISST-related signals removed onto PPT in dust season (Jun.–Jul.); (c)–(d) Regression of TWISST with ENSO-related signals removed onto PPT in dust season (Jun.–Jul.).**



355  
356  
357  
358

**Figure 13: (a)–(b) Regression of ENSO with TWISST-related signals removed onto SoilM in dust season (Jun.–Jul.); (c)–(d) Regression of TWISST with ENSO-related signals removed onto SoilM in dust season (Jun.–Jul.).**



359  
360  
361  
362

**Figure 14: (a)–(b) Regression of ENSO with TWISST-related signals removed onto velocity potential at 850hPa (VP850) and wind in dust season (Jun.–Jul.); (c)–(d) Regression of TWISST with ENSO-related signals removed onto velocity potential at 850hPa (VP850) and wind in dust season (Jun.–Jul.).**

### 363 3.2.3 Pacific Decadal Oscillation

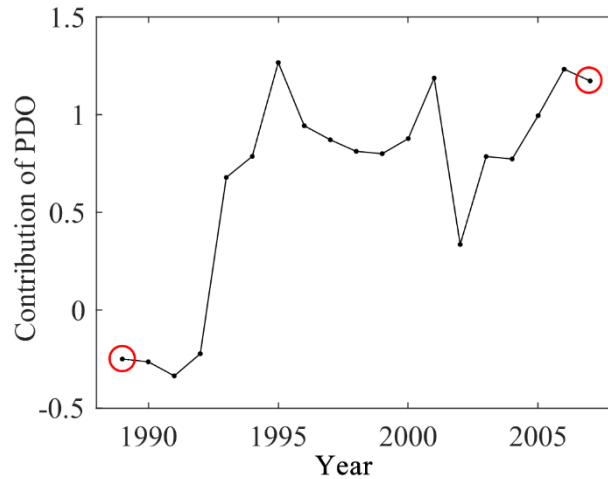
364 It is suggested that the PDO can influence the interannual variability of ISMR by enhancing the  
365 ENSO–ISMR relationship when ENSO and PDO were in-phase, while weakening the relationship when

366 they were out of phase (Dong et al., 2018; Krishnamurthy and Krishnamurthy, 2014). However, it is  
 367 unclear whether PDO is responsible for the shift of the DUCMASS–Niño-3 relationship. Table 2 listed  
 368 the years with different phases of ENSO and PDO as well as years when ENSO and PDO are in (out of)  
 369 phase separately. The correlation coefficient between ENSO and DUCMASS and significance level were  
 370 also given. It demonstrated that the PDO significantly strengthened the correlation between ENSO and  
 371 DUCMASS as the coefficient turned from  $-0.39$  ( $P>0.1$ ) when PDO and ENSO were out of phase to  $-$   
 372  $0.69$  ( $P<0.01$ ) when they were in phase.

373 **Table 2: List of individual and combined wintertime ENSO–PDO years during 1982–2014.**

Events	Phase	
	Positive	Negative
ENSO	1983, 1987, 1988, 1991, 1993–1995, 1998, 2003, 2005, 2007, 2010, 2015, 2016, 2019	1982, 1984–1986, 1989, 1996, 1997, 1999–2001, 2006, 2008, 2009, 2011, 2012, 2014
PDO	1981–1988, 1996–1998, 2001, 2003– 2006, 2010, 2014–2019	1989, 1991, 1995, 1999, 2000, 2002, 2008, 2009, 2011, 2012
ENSO×PDO	1983, 1987–1989, 1998–2000, 2003, 2005, 2008–2012	1982, 1984–1986, 1991, 1995–1997, 2001, 2006, 2014
R (Niño-3 & DUCMASS)	$-0.69$ ( $P<0.01$ )	$-0.39$ ( $P>0.1$ )

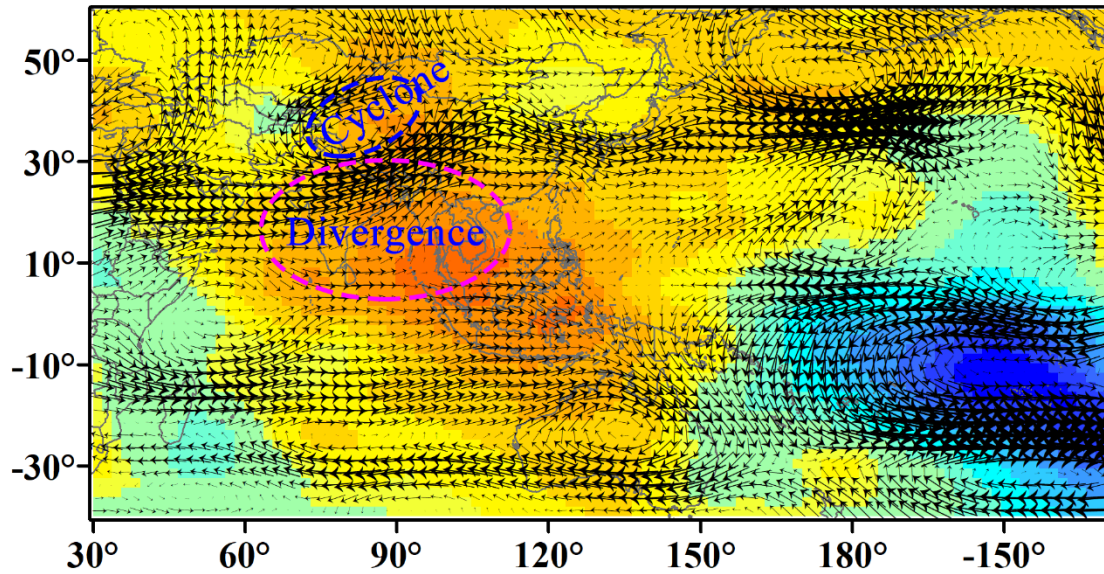
374 Table 2 revealed that P2 includes most of years (8 out of 14) when ENSO and PDO were in-phase,  
 375 i.e., 2000, 2003, 2005, and 2008–2012, while most of the out-of-phase years (8 out of 11) appeared in  
 376 P1, i.e., 1982, 1984–1986, 1991, 1995, 1996, and 1997. Simultaneously, the winter Niño-3 exhibited  
 377 lower correlation with DUCMASS in P1 when most of ENSO years were accompanied with anti-phase  
 378 PDO. In addition, the quantitative contribution of PDO shown in Fig. 15 further confirmed that the PDO  
 379 strengthened the impact of ENSO on DUCMASS in P2 while the contribution was close to 0.0 in P1. All  
 380 those demonstrated that the phase shift of PDO plays an important role in modulating the revolution of  
 381 DUCMASS–Niño-3 relationship.



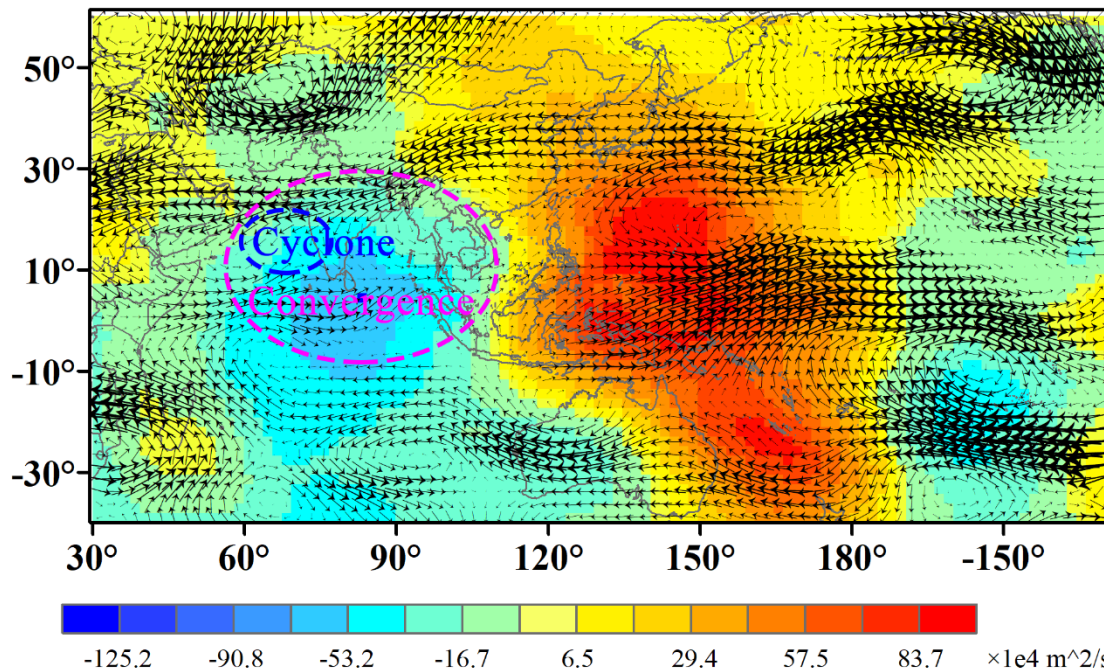
382  
 383 **Figure 15: Sliding contribution of PDO to DUCMASS–Niño-3 relationship. The two circles represented the**  
 384 **15-year window spanning from 1982 to 1996 and 2000 to 2014, respectively.**

385 **Figure 16 revealed the influence mechanism of PDO onto DUCMASS. During P1, the 200hPa**  
 386 **velocity potential in the positive PDO years exhibited a decrease (convergence) over the eastern tropical**  
 387 **Pacific and an increase (divergence) over the tropical Indian Ocean and Indian subcontinent (Fig. 16 (a)).**  
 388 **The upper-level divergence over India and the adjacent seas corresponded to the anomalous ascending**  
 389 **motion, which promoted ISMR and consequently suppressed the dust storms over South Asia.**  
 390 **Meanwhile, an anomalous cyclone developed to the north of India due to the enhanced convection. The**  
 391 **westerlies on the southern flank of the cyclonic anomaly transported wet air from the Arabian Sea to the**  
 392 **northwest of India (Huang et al., 2020), which further inhibited dust emissions. While in the negative**  
 393 **PDO years during P2, the 200hPa velocity potential exhibited a decrease (convergence) over India,**  
 394 **corresponding to an anomalous descending motion, as shown in Fig. 16 (b). This descending flow**  
 395 **suppressed the Indian monsoon convection and rainfall, which consequently enhanced dust emissions.**  
 396 **Similarly, an anomalous cyclone developed over the south of India. The easterlies on the northern flank**  
 397 **of the cyclonic anomaly advected relatively drier air from the Eurasian continent to the northern India**  
 398 **(Parker et al., 2016), which favored dust emissions. The difference of flow movements and their effects**  
 399 **on dust activities between positive and negative PDO years was consistent with that between El Niño**  
 400 **and La Niña years, which further proved that PDO could significantly strengthen the effect of ENSO on**  
 401 **DUCMASS when it was in phase with ENSO.**

**(a) Reg of VP & UV at 200hPa onto PDO in 1982-1996**



**(b) Reg of VP & UV at 200hPa onto PDO in 2000-2014**



402

403 **Figure 16: (a) Regression of summer (Jun.-Jul.) velocity potential at 200hPa onto previous winter PDO**  
404 **(averaged from Nov. to Jan.) overlaid with the average of summer wind in positive PDO years during 1982–**  
405 **1996; (b) Regression of summer velocity potential at 200hPa onto previous winter PDO overlaid with the**  
406 **average of summer wind in negative PDO years during 2000–2014.**

407

**4 Discussion**

408

**4.1 Response of Atlantic SSTA pattern to CT/EM ENSO**

409

**It was reported that the interdecadal shift of tropical Atlantic SSTA pattern was a response to the**

410 multi-year ENSO events (Tokinaga et al., 2019). The multi-year ENSO event, namely continuing ENSO  
 411 (CT ENSO), was a situation where the summer ENSO SSTA continued from the preceding year. Another  
 412 type of ENSO, which was called as emerging ENSO (EM ENSO), was characterized as late Atlantic  
 413 SSTA response that started from June. The CT ENSO primarily dominated during P1, while P2 was  
 414 dominated by EM ENSO (Yang and Huang, 2021). The impact of the two types of ENSO on the shift of  
 415 the DUCMASS–Niño-3 relationship were examined. Table 3 showed that ASGI was significantly  
 416 correlated with Niño-3 in the CT ENSO years, which was not observed in the EM ENSO years.  
 417 Simultaneously, DUCMASS was significantly related to Niño-3 only in the EM ENSO years. The  
 418 composite correlation difference between CT and EM ENSOs was consistent with that between the  
 419 period of P1 and P2, indicating that the shift of Atlantic SSTA pattern, which was prominently modulated  
 420 by the type of ENSO, plays an important role in modulating the DUCMASS–Niño-3 relationship.

421 **Table 3: Correlation between ASGI and Niño-3 as well as DUCMASS in two different phases (\* and \*\*\***  
 422 **indicate the correlations that are significant on a 0.1 and 0.01 level, respectively).**

R	CT ENSO	EM ENSO	P1	P2
ASGI & Niño-3	0.78 (***)	0.19	0.73 (***)	0.46 (*)
DUCMASS & Niño-3	-0.60 (*)	-0.75 (***)	-0.51 (*)	-0.67 (***)

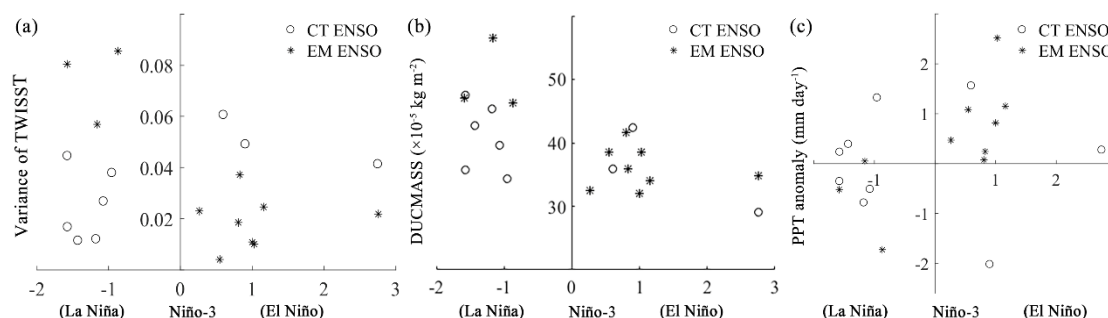
423

#### 424 4.2 Response of Indian ocean SSTA pattern to CT/EM ENSO

425 As discussed in Sect. 3.2.2, ENSO can affect the Indian Ocean SST and the Indian Ocean variability  
 426 can also modulate the ENSO variability (Kug et al., 2005; Wu and Kirtman, 2004; Yu et al., 2002). It is  
 427 known that during CT ENSO years, the ENSO event in summer primarily starts from the preceding  
 428 winter, while in EM ENSO years, the ENSO event mainly emerges in late spring (Yang and Huang, 2021).  
 429 Correspondingly, the associated Indian Ocean SST oscillation also varies in these two different ENSO  
 430 years. In order to explore whether the different types of ENSO impacted the DUCMASS over the  
 431 northwestern South Asia through adjusting the duration of the temperature anomaly, we compared the  
 432 SST and the variance of the monthly SSTA from (–1) Sep. to (0) May over the tropical western Indian  
 433 ocean (TWISSTA).

434 Figure 17 (a) showed that the variances in the EM La Niña years were generally larger than that in

435 the CT La Niña years, while the variances in the EM El Niño years were generally smaller than that in  
 436 the CT El Niño years. Concurrently, the difference of DUCMASS in El Niño and La Niña years was  
 437 obvious in the EM ENSO period with higher values appeared in La Niña years (Fig. 17 (b)). However,  
 438 in the CT ENSO period, no significant difference was observed between El Niño and La Niña years.  
 439 Therefore, it is hypothesized that the EM ENSO conditions, which was associated with higher TWISST  
 440 variance, were more favorable to trigger the variation of DUCMASS. Yang and Huang (2021) reported  
 441 that P1 was primarily dominated by CT ENSOs while EM ENSOs primarily controlled during P2.  
 442 Combined with abovementioned hypothesis, the correlation between DUCMASS and Niño-3 should be  
 443 higher in P2, which was consistent with the interdecadal change of this relationship. Figure 17 (c) further  
 444 revealed the influence mechanism of TWISSTA onto DUCMASS. It showed that compared to CT ENSO  
 445 type, the difference of PPT between El Niño and La Niña years was more significant in the EM ENSO  
 446 years, in addition, the PPT in La Niña years (with high TWISSTA variance) was lower than that in El  
 447 Niño years (with low TWISSTA variance), which was contrary to the difference of DUCMASS between  
 448 those two types of ENSO years. While when other atmospheric factors were considered, such as land  
 449 cover and winds at multi-layers, no similar change was observed. This indicated that the Indian Ocean  
 450 SSTA, which was also remarkably modulated by the type of ENSO, impacted DUCMASS by adjusting  
 451 the PPT and further influenced the relationship between ENSO and DUCMASS.



452  
 453 **Figure 17: Scatter diagram between (a) variance of the monthly TWISSTA from (-1) Sep. to (0) May, (b)**  
 454 **DUCMASS, and (c) PPT anomaly and Niño-3 index separately for continuing (CT) and emerging (EM) ENSO.**

### 455 4.3 Uncertainty in analyzing the contribution of the influence factors

456 The contributions of those abovementioned factors to the interdecadal shift of ENSO-DUCMASS  
 457 relationship were analyzed based on the linear regression model. However, the linear regression model  
 458 would definitely bring uncertainty to the results (Guo et al., 2017) and may not be sufficient to verify the

459 cause and effect. Thus, the numerical models are suggested for future research to quantify the  
460 contribution of those factors to the shift of ENSO–DUCMASS relationship. However, before such  
461 quantitative study the regression analysis is indispensable to identify the possible driving factors. In this  
462 context, it is undeniable that this study provides new sights to the dust storm-related numerical simulation  
463 by taking account of the teleconnections and their influence mechanisms.

464 In addition, while analyzing the effects of different types of ENSO event, we compared the variance  
465 of TWISST and DUCMASS under the two types of ENSO periods, as shown in Fig. 17. It showed that  
466 only eight EM ENSO years were identified and the number of PDO years that were in or out of phase  
467 with ENSO were also insufficient. The statistical results acquired from the insufficient number of  
468 samples could also be explained by the random events (Pallikari, 2004). In order to verify this conclusion,  
469 we calculated the interannual correlation between the variance of TWISST and DUCMASS from 1982  
470 to 2014. Even so, the significant interannual correlation does not guarantee the significant link between  
471 different types of ENSO. Therefore, longer time series with valid samples (i.e., CT/EM ENSO and PDO  
472 years) are needed to further validate the influence of ENSO types on the ENSO–DUCMASS relationship  
473 in the future. Alternatively, using numerical model to simulate the teleconnection pattern of ENSO over  
474 South Asia under different types of ENSO is also favorable.

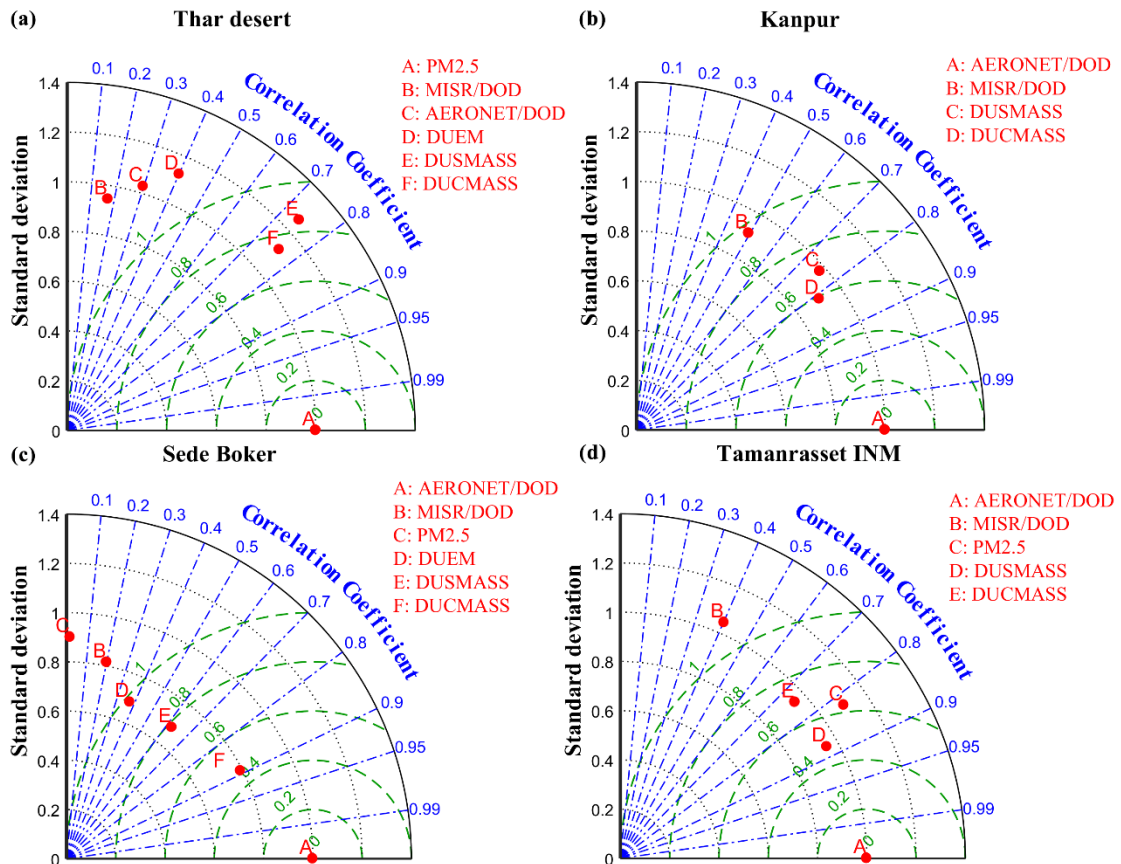
475 Except for the large-scale atmospheric circulation, the anthropogenic land-use management could  
476 also play an important role in the interdecadal variability of ENSO–DUCMASS relationship (Kumar et  
477 al., 1999), which should be considered in the future researches.

478 The dust activities analyzed in this study were from the dust season, i.e., Jun.–Jul., which were part  
479 of monsoon season (Jun.–Sep.) (Babu et al., 2013), however, the dust activities during pre-monsoon  
480 season (Mar.–May or Apr.–May) were also a hot topic (Babu et al., 2013; Lakshmi et al., 2017, 2019).  
481 Therefore, we analyzed the interdecadal change of the ENSO impact on DUCMASS during dust season  
482 (Jun.–Jul.) and pre-monsoon (Mar.–May or Apr.–May) separately, to find that the significant interdecadal  
483 change occurred only when the DUCMASS during dust season was considered. As for that during pre-  
484 monsoon season, there should be some other factors that influenced its interdecadal change, which will  
485 be discussed in the future study.

#### 486 4.4 Precision validation of MERRA-2 dust concentration dataset



487 It is known that the nonspherical aerosol optical depth retrieved from satellite, concentration of  
488 PM<sub>2.5</sub>/PM<sub>10</sub> and coarse mode aerosol optical depth acquired from observation stations represent  
489 extinction characteristics of dust aerosols in the whole atmospheric column, thus they can be used to  
490 validate the dust column concentration datasets but not appropriate for the validation of dust emission,  
491 which reflect the dust loading lifted from ground. The dust dataset used in this study was the dust column  
492 concentration “Dust Column Mass Density-PM<sub>2.5</sub>”, thus the PM<sub>2.5</sub>, coarse mode aerosol optical depth  
493 acquired from AERONET (AERONET/DOD), and nonspherical aerosol optical depth retrieved from  
494 MISR (MISR/DOD) was utilized to validate the precision of DUCMASS dataset. The time coverage and  
495 continuity of satellite and observation-based products lagged behind the MERRA-2 datasets, thus only  
496 several stations over the dust belt with relatively longer time series were chosen. They were Kanpur (26.5°  
497 N, 80.2° E. Time span: 2001–2021), Sede Boker (30.9° N, 34.8° E. Time span: 2007–2019), and  
498 Tamanrasset INM (22.8° N, 5.5° E. Time span: 2007–2019). The MISR/DOD, PM<sub>2.5</sub>, and dust variables  
499 from MERRA-2 were the regional average within 1° of the corresponding station. No dust emission was  
500 observed over the Kanpur and Tamanrasset INM station. Besides, the datasets over the study area  
501 (represented by Thar desert in Fig. 18 (a)) were also accounted and the AERONET/DOD was obtained  
502 from the nearest Kanpur station. For the study area, PM<sub>2.5</sub> was chosen as the reference dataset (A) because  
503 the study area was not overlapped with the Kanpur station, while AERONET/DOD was chosen as the  
504 reference data for other stations.



505

506

**Figure 18: Precision validation of MERRA-2 dust concentration datasets**

507

Figure 18 (a) compared the precision of MISR/DOD, AERONET/DOD, dust emission (DUEM),

508

surface dust mass concentration (DUSMASS), and DUCMASS with that of PM<sub>2.5</sub>, it showed that no

509

significant correlation was observed between AERONET/DOD and PM<sub>2.5</sub> because this study area did not

510

coincide with the Kanpur station. However, the correlations between PM<sub>2.5</sub> and DUSMASS as well as

511

DUCMASS were significant ( $R>0.7$ ,  $RMSE<0.9$ ) and stronger than that between PM<sub>2.5</sub> and DUEM.

512

Figure 18 (b) showed the precision of MISR/DOD, DUSMASS, and DUCMASS compared with

513

AERONET/DOD over the Kanpur station. The results indicated that both DUSMASS and DUCMASS

514

were significantly correlated with AERONET/DOD ( $R>0.7$ ,  $RMSE<0.8$ ). In addition, the comparison

515

results over the other two stations also indicated that DUSMASS and DUCMASS were significantly

516

correlated with AERONET/DOD, while the relationship between DUEM and AERONET/DOD was

517

weak, as shown in Figs. 18 (c)–(d). The above results demonstrated that the DUCMASS from MERRA-

518

2 was strongly consistent with MISR/DOD, AERONET/DOD, and PM<sub>2.5</sub>, indicating that the DUCMASS

519

datasets used in this study were with high precision.

## 520 **5 Conclusions**

521 In the study, we revealed the interdecadal change of the ENSO impact on DUCMASS over the  
522 northwestern South Asia from 1982 to 2014, and further investigated the factors contributing to the shifts  
523 of the responses of DUCMASS to the wintertime ENSO. It was found that the ENSO–DUCMASS  
524 relationship shifted from weak negative relation during 1982–1996 to significant negative correlation  
525 during 2000–2014. The change of Atlantic and Indian ocean SSTA pattern weakened the impact of  
526 wintertime ENSO on dust activities over the northwestern South Asia during 1982–1996, while PDO  
527 tended to strengthen ENSO’s effect on dust activities when it was in phase with ENSO. Both the Atlantic  
528 and Indian Ocean SSTA patterns were modulated by the duration of ENSO events (i.e., continuing and  
529 emerging ENSO). The current results are based solely on the linear regression, and further studies  
530 integrating numerical models and longer time series are needed to validate the results. Nevertheless, this  
531 study indeed found multiple large-scale factors that could impact the interdecadal interaction between  
532 ENSO and dust activities over the northwestern South Asia. Given that it is possible to forecast the  
533 change of some large-scale atmospheric circulation patterns, the results of this study could provide new  
534 insight to the prediction of dust storm trend in the near future based on the variability of ENSO–  
535 DUCMASS relationship.

## 536 **Data availability**

537 The data can be downloaded for free from the corresponding website which were listed in the text.

## 538 **Author contribution**

539 L.S. designed the study, performed the analysis with feedback from J.Z. and F.Y., and wrote the  
540 paper that was reviewed by J.Z., F.Y., D.Z., J.W., X.M., and Y.L.. All the authors discussed the results.

## 541 **Competing interests**

542 The authors declare that they have no conflict of interest.

## 543 **Acknowledgments**

544 The authors would like to thank the Modern-Era Retrospective Analysis for Research and  
545 Applications, version 2 (MERRA-2) for providing the surface dust mass concentration, wind speed and  
546 planetary boundary layer height, the National Oceanic and Atmospheric Administration (NOAA) for  
547 providing the SST, the Hadley Centre Climate Research Unit for the land-surface temperature and  
548 precipitation, the National Aeronautics and Space Administration (NASA) for the NDVI, and the Climate  
549 Predict Center of National Oceanic and Atmospheric Administration (NOAA/CPC) for the large-scale  
550 climate indices.

551 This work was supported by the Strategic Priority Research Program of the Chinese Academy of  
552 Sciences-A (No. XDA19030402) and the National Natural Science Foundation of China (No. 42071425).

### 553 **References**

554 Abish, B. and Mohanakumar, K.: Absorbing aerosol variability over the Indian subcontinent and its  
555 increasing dependence on ENSO, *Glob. Planet. Change*, 106, 13–19,  
556 doi:10.1016/j.gloplacha.2013.02.007, 2013.

557 Ashok, K., Behera, S. K., Rao, S. A., Weng, H. and Yamagata, T.: El Nino Modoki and its possible  
558 teleconnection, *J. Geophys. Res.*, 112, C11007, 2007.

559 Augustyn, A., Zeidan, A., Zelazko, A., Eldridge, A., McKenna, A., Tikkanen, A., Gadzikowski, A.,  
560 Schreiber, B. A., Duignan, B., Mahajan, D., Prommet, D., Goldstein, E. and Rodriguez, E.: Thar  
561 Desert, *Encycl. Br.* [online] Available from: <https://www.britannica.com/place/Thar-Desert>, 2019.

562 Avila, A.: The chemical composition of dust transported in red rains—its contribution to the  
563 biogeochemical cycle of a holm oak forest in Catalonia (Spain), *Atmos. Environ.*, 32(2), 179–191,  
564 1998.

565 Babu, S. S., Manoj, M. R., Moorthy, K. K., Gogoi, M. M., Nair, V. S., Kompalli, S. K., Satheesh, S. K.,  
566 Niranjana, K., Ramagopal, K., Bhuyan, P. K. and Singh, D.: Trends in aerosol optical depth over  
567 Indian region: Potential causes and impact indicators, *J. Geophys. Res. Atmos.*, 118(20), 11,794-  
568 11,806, doi:10.1002/2013JD020507, 2013.

569 Banerjee, P. and Kumar, S. P.: ENSO modulation of interannual variability of dust aerosols over the  
570 northwest Indian Ocean, *J. Clim.*, 29(4), 1391–1415, doi:10.1175/JCLI-D-15-0039.1, 2016.

571 Banerjee, P., Satheesh, S. K., Moorthy, K. K., Nanjundiah, R. S. and Nair, V. S.: Long-range transport  
572 of mineral dust to the northeast Indian Ocean: Regional versus remote sources and the implications,  
573 *J. Clim.*, 32(5), 1525–1549, doi:10.1175/JCLI-D-18-0403.1, 2019.

574 Behrooz, R. D., Esmaili-Sari, A., Bahramifar, N. and Kaskaoutis, D. G.: Analysis of the TSP, PM10  
575 concentrations and water-soluble ionic species in airborne samples over Sistan, Iran during the  
576 summer dusty period, *Atmos. Pollut. Res.*, 8(3), 403–417, 2017.

577 Bollasina, M. A., Ming, Y. and Ramaswamy, V.: Anthropogenic aerosols and the weakening of the south  
578 asian summer monsoon, *Science (80-. )*, 334(6055), 502–505, doi:10.1126/science.1204994, 2011.

579 Bozlaker, A., Prospero, J. M., Fraser, M. P. and Chellam, S.: Quantifying the contribution of long-range  
580 saharan dust transport on particulate matter concentrations in Houston, Texas, using detailed  
581 elemental analysis, *Environ. Sci. Technol.*, 47(18), 10179–10187, doi:10.1021/es4015663, 2013.

582 Buchard, V., Randles, C. A., da Silva, A. M., Darmenov, A., Colarco, P. R., Govindaraju, R., Ferrare,  
583 R., Hair, J., Beyersdorf, A. J., Ziemba, L. D. and Yu, H.: The MERRA-2 aerosol reanalysis, 1980  
584 onward. Part II: Evaluation and case studies, *J. Clim.*, 30(17), 6851–6872, doi:10.1175/JCLI-D-16-  
585 0613.1, 2017.

586 Cai, W., Borlace, S., Lengaigne, M., Van Rensch, P., Collins, M., Vecchi, G., Timmermann, A., Santoso,  
587 A., Mcphaden, M. J., Wu, L., England, M. H., Wang, G., Guilyardi, E. and Jin, F. F.: Increasing  
588 frequency of extreme El Niño events due to greenhouse warming, *Nat. Clim. Chang.*, 4(2), 111–116,  
589 doi:10.1038/nclimate2100, 2014.

590 Chauhan, S. S.: Desertification control and management of land degradation in the Thar desert of India,  
591 *Environmentalist*, 23(3), 219–227, doi:10.1023/B:ENVR.0000017366.67642.79, 2003.

592 Chen, Y.-S., Sheen, P.-C., Chen, E.-R., Liu, Y.-K., Wu, T.-N. and Yang, C.-Y.: Effects of Asian dust  
593 storm events on daily mortality in Taipei, Taiwan., *Environ. Res.*, 95(2), 151–155,  
594 doi:10.1016/j.envres.2003.08.008, 2004.

595 Cherchi, A. and Navarra, A.: Influence of ENSO and of the Indian Ocean Dipole on the Indian summer  
596 monsoon variability, *Clim. Dyn.*, 41(1), 81–103, doi:10.1007/s00382-012-1602-y, 2013.

597 Clark, C. O., Cole, J. E. and Webster, P. J.: Indian Ocean SST and Indian summer rainfall: Predictive  
598 relationships and their decadal variability, *J. Clim.*, 13(14), 2503–2519, doi:10.1175/1520-

599 0442(2000)013<2503:IOSAIS>2.0.CO;2, 2000.

600 Dong, B., Dai, A., Vuille, M. and Timm, O. E.: Asymmetric modulation of ENSO teleconnections by  
601 the interdecadal Pacific oscillation, *J. Clim.*, 31(18), 7337–7361, doi:10.1175/JCLI-D-17-0663.1,  
602 2018.

603 Du, Y., Xie, S. P., Huang, G. and Hu, K.: Role of air-sea interaction in the long persistence of El Niño-  
604 induced north Indian Ocean warming, *J. Clim.*, 22(8), 2023–2038, doi:10.1175/2008JCLI2590.1,  
605 2009.

606 Easterling, D. R. and Wehner, M. F.: Is the climate warming or cooling?, *Geophys. Res. Lett.*, 36(8), 4–  
607 6, doi:10.1029/2009GL037810, 2009.

608 Erel, Y., Dayan, U., Rabi, R., Rudich, Y. and Stein, M.: Trans boundary transport of pollutants by  
609 atmospheric mineral dust, *Environ. Sci. Technol.*, 40(9), 2996–3005, doi:10.1021/es051502l, 2006.

610 Fyfe, J. C., Merryfield, W. J., Kharin, V., Boer, G. J., Lee, W. S. and Von Salzen, K.: Skillful predictions  
611 of decadal trends in global mean surface temperature, *Geophys. Res. Lett.*, 38(22), 1–5,  
612 doi:10.1029/2011GL049508, 2011.

613 Fyfe, J. C., Gillett, N. P. and Zwiers, F. W.: Overestimated global warming over the past 20 years, *Nat.*  
614 *Clim. Chang.*, 3(9), 767–769, doi:10.1038/nclimate1972, 2013.

615 Gelaro, R., McCarty, W., Suárez, M. J., Todling, R., Molod, A., Takacs, L., Randles, C. A., Darmenov,  
616 A., Bosilovich, M. G., Reichle, R., Wargan, K., Coy, L., Cullather, R., Draper, C., Akella, S., Buchard,  
617 V., Conaty, A., da Silva, A. M., Gu, W., Kim, G. K., Koster, R., Lucchesi, R., Merkova, D., Nielsen,  
618 J. E., Partyka, G., Pawson, S., Putman, W., Rienecker, M., Schubert, S. D., Sienkiewicz, M. and Zhao,  
619 B.: The modern-era retrospective analysis for research and applications, version 2 (MERRA-2), *J.*  
620 *Clim.*, 30(14), 5419–5454, doi:10.1175/JCLI-D-16-0758.1, 2017.

621 Graham, N. E.: Decadal-scale climate variability in the tropical and North Pacific during the 1970s and  
622 1980s: observations and model results, *Clim. Dyn.*, 10(3), 135–162, doi:10.1007/BF00210626, 1994.

623 Guo, H., Wang, X. and Gao, Z.: Uncertain linear regression model and its application, *J. Intell. Manuf.*,  
624 28(3), 559–564, doi:10.1007/s10845-014-1022-4, 2017.

625 He, L., Lin, A., Chen, X., Zhou, H., Zhou, Z. and He, P.: Assessment of MERRA-2 Surface PM<sub>2.5</sub> over  
626 the Yangtze River Basin: Ground-based verification, spatiotemporal distribution and meteorological

627 dependence, *Remote Sens.*, 11(4), 460, doi:10.3390/rs11040460, 2019.

628 He, S. and Wang, H.: Oscillating relationship between the East Asian Winter Monsoon and ENSO, *J.*  
629 *Clim.*, 26(24), 9819–9838, doi:10.1175/JCLI-D-13-00174.1, 2013.

630 Hirahara, S., Ishii, M. and Fukuda, Y.: Centennial-scale sea surface temperature analysis and its  
631 uncertainty, *J. Clim.*, 27(1), 57–75, doi:10.1175/JCLI-D-12-00837.1, 2014.

632 Hu, S. and Fedorov, A. V.: The extreme El Niño of 2015–2016 and the end of global warming hiatus,  
633 *Geophys. Res. Lett.*, 44(8), 3816–3824, doi:10.1002/2017GL072908, 2017.

634 Huang, X., Zhou, T., Turner, A., Dai, A., Chen, X., Clark, R., Jiang, J., Man, W., Murphy, J., Rostron,  
635 J., Wu, B., Zhang, L., Zhang, W. and Zou, L.: The recent decline and recovery of Indian summer  
636 monsoon rainfall: Relative roles of external forcing and internal variability, *J. Clim.*, 33(12), 5035–  
637 5060, doi:10.1175/JCLI-D-19-0833.1, 2020.

638 Jin, Q. and Wang, C.: The greening of Northwest Indian subcontinent and reduction of dust abundance  
639 resulting from Indian summer monsoon revival, *Sci. Rep.*, 8(1), 1–9, doi:10.1038/s41598-018-  
640 23055-5, 2018.

641 Jin, Q., Wei, J., Pu, B., Yang, Z. L. and Parajuli, S. P.: High Summertime Aerosol Loadings Over the  
642 Arabian Sea and Their Transport Pathways, *J. Geophys. Res. Atmos.*, 123(18), 10,568–10,590,  
643 doi:10.1029/2018JD028588, 2018.

644 Kaiser, J. and Granmar, M.: Mounting Evidence Indicts Fine-Particle Pollution, *Science* (80-. ),  
645 307(5717), 1858–1861, 2005.

646 Kinter, I. L., Miyakoda, K. and Yang, S.: Recent change in the connection from the Asian monsoon to  
647 ENSO, *J. Clim.*, 15(10), 1203–1215, doi:10.1175/1520-0442(2002)015<1203:RCITCF>2.0.CO;2,  
648 2002.

649 Kosaka, Y. and Xie, S. P.: Recent global-warming hiatus tied to equatorial Pacific surface cooling, *Nature*,  
650 501(7467), 403–407, doi:10.1038/nature12534, 2013.

651 Krishnamurthy, L. and Krishnamurthy, V.: Influence of PDO on South Asian summer monsoon and  
652 monsoon-ENSO relation, *Clim. Dyn.*, 42(9–10), 2397–2410, doi:10.1007/s00382-013-1856-z, 2014.

653 Krishnamurthy, V. and Kirtman, B. P.: Variability of the Indian Ocean: Relation to monsoon and ENSO,  
654 *Q. J. R. Meteorol. Soc.*, 129(590), 1623–1646, doi:10.1256/qj.01.166, 2003.

655 Kucharski, F., Bracco, A., Yoo, J. H. and Molteni, F.: Low-frequency variability of the Indian monsoon-  
656 ENSO relationship and the tropical Atlantic: The “weakening” of the 1980s and 1990s, *J. Clim.*,  
657 20(16), 4255–4266, doi:10.1175/JCLI4254.1, 2007.

658 Kug, J. S., An, S. Il, Jin, F. F. and Kang, I. S.: Preconditions for El Niño and La Niña onsets and their  
659 relation to the Indian Ocean, *Geophys. Res. Lett.*, 32(5), 1–5, doi:10.1029/2004GL021674, 2005.

660 Kumar, K. K., Rajagopalan, B. and Cane, M. A.: On the weakening relationship between the Indian  
661 monsoon and ENSO, *Science* (80-. ), 284(5423), 2156–2159, doi:10.1126/science.284.5423.2156,  
662 1999.

663 Lakshmi, N. B., Nair, V. S. and Suresh Babu, S.: Vertical structure of aerosols and mineral dust over the  
664 Bay of Bengal from multisatellite observations, *J. Geophys. Res. Atmos.*, 122(23), 12,845–12,861,  
665 doi:10.1002/2017JD027643, 2017.

666 Lakshmi, N. B., Babu, S. S. and Nair, V. S.: Recent Regime Shifts in Mineral Dust Trends over South  
667 Asia from Long-Term CALIPSO Observations, *IEEE Trans. Geosci. Remote Sens.*, 57(7), 4485–  
668 4489, doi:10.1109/TGRS.2019.2891338, 2019.

669 Lee, Y. G., Kim, J., Ho, C. H., An, S. Il, Cho, H. K., Mao, R., Tian, B., Wu, D., Lee, J. N., Kalashnikova,  
670 O., Choi, Y. and Yeh, S. W.: The effects of ENSO under negative AO phase on spring dust activity  
671 over northern China: An observational investigation, *Int. J. Climatol.*, 35(6), 935–947,  
672 doi:10.1002/joc.4028, 2015.

673 Li, T., Zhang, Y., Lu, E. and Wang, D.: Relative role of dynamic and thermodynamic processes in the  
674 development of the Indian Ocean dipole: An OGCM diagnosis, *Geophys. Res. Lett.*, 29(23),  
675 doi:10.1029/2002GL015789, 2002.

676 Liu, J., Wu, D., Liu, G., Mao, R., Chen, S., Ji, M., Fu, P., Sun, Y., Pan, X., Jin, H., Zhou, Y. and Wang,  
677 X.: Impact of Arctic amplification on declining spring dust events in East Asia, *Clim. Dyn.*, 54(3–4),  
678 1913–1935, doi:10.1007/s00382-019-05094-4, 2020.

679 Mahowald, N. M., Kloster, S., Engelstaedter, S., Moore, J. K., Mukhopadhyay, S., McConnell, J. R.,  
680 Albani, S., Doney, S. C., Bhattacharya, A., Curran, M. A. J., Flanner, M. G., Hoffman, F. M.,  
681 Lawrence, D. M., Lindsay, K., Mayewski, P. A., Neff, J., Rothenberg, D., Thomas, E., Thornton, P.  
682 E. and Zender, C. S.: Observed 20th century desert dust variability: Impact on climate and



683 biogeochemistry, *Atmos. Chem. Phys.*, 10(22), 10875–10893, doi:10.5194/acp-10-10875-2010,  
684 2010.

685 Nitta, T. and Yamada, S.: Recent warming of tropical sea surface temperature and its relationship to the  
686 Northern Hemisphere circulation, *J. Meteorol. Soc. Japan*, 67(3), 375–383,  
687 doi:10.2151/jmsj1965.67.3\_375, 1989.

688 Osborn, T. J., Jones, P. D., Lister, D. H., Morice, C. P., Simpson, I. R., Winn, J. P., Hogan, E. and Harris,  
689 I. C.: Land Surface Air Temperature Variations Across the Globe Updated to 2019: The CRUTEM5  
690 Data Set, *J. Geophys. Res. Atmos.*, 126(2), doi:10.1029/2019JD032352, 2021.

691 Pallikari, F.: On the false hypothesis of psi-mediated shift of statistical average in tests with random  
692 number generators, in *The Parapsychological Association Convention 2004*, pp. 157–171., 2004.

693 Parker, D. J., Willetts, P., Birch, C., Turner, A. G., Marsham, J. H., Taylor, C. M., Kolusu, S. and Martin,  
694 G. M.: The interaction of moist convection and mid-level dry air in the advance of the onset of the  
695 Indian monsoon, *Q. J. R. Meteorol. Soc.*, 142(699), 2256–2272, doi:10.1002/qj.2815, 2016.

696 Poulsen, O. M., Breum, N. O., Ebbehoj, N., Hansen, A. M., Ivens, U. I., van Lelieveld, D., Malmros, P.,  
697 Matthiasen, L., Nielsen, B. H. and Nielsen, E. M.: Sorting and recycling of domestic waste. Review  
698 of occupational health problems and their possible causes., *Sci. Total Environ.*, 168(1), 33–56, 1995.

699 Prospero, J. M. and Nees, R. T.: Impact of the North African drought and El Niño on mineral dust in the  
700 Barbados trade winds, *Nature*, 320(6064), 735–738, doi:10.1038/320735a0, 1986.

701 Randles, C. A., Sliva, A. M. da, Buchard, V., Colarco, P., Armenov, A. and Govindaraju, R.: The  
702 MERRA-2 Aerosol Reanalysis, 1980 Onward. Part I: System Description and Data Assimilation  
703 Evaluation, *J. Clim.*, 30(17), 6823–6850, doi:10.1175/JCLI-D-16-0609.1, 2017.

704 Rayner, N. A., Parker, D. E., Horton, E. B., Folland, C. K., Alexander, L. V., Rowell, D. P., Kent, E. C.  
705 and Kaplan, A.: Global analyses of sea surface temperature, sea ice, and night marine air temperature  
706 since the late nineteenth century, *J. Geophys. Res. Atmos.*, 108(D14), 4407,  
707 doi:10.1029/2002jd002670, 2003.

708 Razakov, R. M. and Kosnazarov, K. A.: Dust and salt transfer from the exposed bed of the Aral Sea and  
709 measures to decrease its environmental impact, in *The Aral Sea Basin*, edited by P. P. Micklin and  
710 W. D. Williams, pp. 95–102, Springer, Berlin, Heidelberg., 1996.

711 Richon, C., Dutay, J., Dulac, F. and Wang, R.: Modeling the biogeochemical impact of atmospheric  
712 phosphate deposition from desert dust and combustion sources to the Mediterranean Sea,  
713 *Biogeosciences*, 15(8), 2499–2524, doi:10.5194/bg-2017-242, 2018.

714 Rienecker, M. M., Suarez, M. J., Gelaro, R., Todling, R., Bacmeister, J., Liu, E., Bosilovich, M. G.,  
715 Schubert, S. D., Takacs, L., Kim, G. K., Bloom, S., Chen, J., Collins, D., Conaty, A., Da Silva, A.,  
716 Gu, W., Joiner, J., Koster, R. D., Lucchesi, R., Molod, A., Owens, T., Pawson, S., Pegion, P., Redder,  
717 C. R., Reichle, R., Robertson, F. R., Ruddick, A. G., Sienkiewicz, M. and Woollen, J.: MERRA:  
718 NASA’s modern-era retrospective analysis for research and applications, *J. Clim.*, 24(14), 3624–  
719 3648, doi:10.1175/JCLI-D-11-00015.1, 2011.

720 Sabeerali, C. T., Ajayamohan, R. S., Bangalath, H. K. and Chen, N.: Atlantic Zonal Mode: An Emerging  
721 Source of Indian Summer Monsoon Variability in a Warming World, *Geophys. Res. Lett.*, 46(8),  
722 4460–4467, doi:10.1029/2019GL082379, 2019.

723 Sanchez de la Campa, A., Garcia-Salamanca, A., Solano, J., de la Rosa, J. and Ramos, J.-L.: Chemical  
724 and microbiological characterization of atmospheric particulate matter during an intense African dust  
725 event in Southern Spain., *Environ. Sci. Technol.*, 47(8), 3630–3638, doi:10.1021/es3051235, 2013.

726 Schulz, M., Prospero, J. M., Baker, A. R., Dentener, F., Ickes, L., Liss, P. S., Mahowald, N. M., Nickovic,  
727 S., García-Pando, C. P., Rodríguez, S., Sarin, M., Tegen, I. and Duce, R. A.: Atmospheric Transport  
728 and Deposition of Mineral Dust to the Ocean: Implications for Research Needs, *Environ. Sci.*  
729 *Technol.*, 46(19), 10390–10404, doi:10.1021/es300073u, 2012.

730 Singh, R. P., Prasad, A. K., Kayetha, V. K. and Kafatos, M.: Enhancement of oceanic parameters  
731 associated with dust storms using satellite data, *J. Geophys. Res.*, 113, C11008,  
732 doi:10.1029/2008JC004815, 2008.

733 Srivastava, G., Chakraborty, A. and Nanjundiah, R. S.: Multidecadal see-saw of the impact of ENSO on  
734 Indian and West African summer monsoon rainfall, *Clim. Dyn.*, 52(11), 6633–6649,  
735 doi:10.1007/s00382-018-4535-2, 2019.

736 Storch, H. von and Zwiers, F. W.: *Statistical Analysis in Climate Research*, Cambridge University Press,  
737 Cambridge., 1999.

738 Tokinaga, H., Richter, I. and Kosaka, Y.: ENSO Influence on the Atlantic Niño, Revisited: Multi-Year

739 versus Single-Year ENSO Events, *J. Clim.*, 32(14), 4585–4600, 2019.

740 Trenberth, K. E. and Hurrell, J. W.: Decadal atmosphere-ocean variations in the Pacific, *Clim. Dyn.*, 9(6),  
741 303–319, doi:10.1007/BF00204745, 1994.

742 Trenberth, K. E., Dai, A., Van Der Schrier, G., Jones, P. D., Barichivich, J., Briffa, K. R. and Sheffield,  
743 J.: Global warming and changes in drought, *Nat. Clim. Chang.*, 4(1), 17–22,  
744 doi:10.1038/nclimate2067, 2014.

745 Veselovskii, I., Goloub, P., Podvin, T., Tanre, D., Da Silva, A., Colarco, P., Castellanos, P., Korenskiy,  
746 M., Hu, Q., Whiteman, D. N., Pérez-Ramírez, D., Augustin, P., Fourmentin, M. and Kolgotin, A.:  
747 Characterization of smoke and dust episode over West Africa: Comparison of MERRA-2 modeling  
748 with multiwavelength Mie-Raman lidar observations, *Atmos. Meas. Tech.*, 11(2), 949–969,  
749 doi:10.5194/amt-11-949-2018, 2018.

750 Wang, B., Wu, R. and Li, T.: Atmosphere-warm ocean interaction and its impacts on Asian-Australian  
751 monsoon variation, *J. Clim.*, 16(8), 1195–1211, doi:10.1175/1520-  
752 0442(2003)16<1195:AOIAII>2.0.CO;2, 2003.

753 Wang, L., Chen, W. and Huang, R.: Interdecadal modulation of PDO on the impact of ENSO on the east  
754 Asian winter monsoon, *Geophys. Res. Lett.*, 35(20), doi:10.1029/2008GL035287, 2008.

755 Wang, S., Huang, J., He, Y. and Guan, Y.: Combined effects of the Pacific Decadal Oscillation and El  
756 Niño-Southern Oscillation on Global Land Dry-Wet Changes, *Sci. Rep.*, 4, 6651,  
757 doi:10.1038/srep06651, 2014.

758 Watanabe, M. and Jin, F. F.: Role of Indian Ocean warming in the development of Philippine Sea  
759 anticyclone during ENSO, *Geophys. Res. Lett.*, 29(10), 1161–1164, doi:10.1029/2001gl014318,  
760 2002.

761 Watanabe, M., Shiogama, H., Tatebe, H., Hayashi, M., Ishii, M. and Kimoto, M.: Contribution of natural  
762 decadal variability to global warming acceleration and hiatus, *Nat. Clim. Chang.*, 4(10), 893–897,  
763 doi:10.1038/nclimate2355, 2014.

764 Weare, B. C., Navato, A. R. and Newell, R. E.: Empirical orthogonal analysis of Pacific sea surface  
765 temperatures, *J. Phys. Oceanogr.*, 6(5), 671–678, 1976.

766 Weng, H., Ashok, K., Behera, S. K., Rao, S. A. and Yamagata, T.: Impacts of recent El Niño Modoki on

767 dry/wet conditions in the Pacific rim during boreal summer, *Clim. Dyn.*, 29(2–3), 113–129,  
768 doi:10.1007/s00382-007-0234-0, 2007.

769 Wu, R. and Kirtman, B. P.: Understanding the impacts of the Indian ocean on ENSO variability in a  
770 coupled GCM, *J. Clim.*, 17(20), 4019–4031, doi:10.1175/1520-  
771 0442(2004)017<4019:UTIOTI>2.0.CO;2, 2004.

772 Xi, X. and Sokolik, I. N.: Dust interannual variability and trend in Central Asia from 2000 to 2014 and  
773 their climatic linkages, *J. Geophys. Res. Atmos.*, 120(23), 12175–12191, doi:10.1038/175238c0,  
774 2016.

775 Yang, S. and Jiang, X.: Prediction of Eastern and Central Pacific ENSO Events and Their Impacts on  
776 East Asian Climate by the NCEP Climate Forecast System, *J. Clim.*, 27(12), 4451–4472,  
777 doi:10.1175/JCLI-D-13-00471.1, 2014.

778 Yang, X. and Huang, P.: Restored relationship between ENSO and Indian summer monsoon rainfall  
779 around 1999/2000, *Innov.*, 2(2), 100102, doi:10.1016/j.xinn.2021.100102, 2021.

780 Yu, J.-Y., Mechoso, C. R., McWilliams, J. C. and Arakawa, A.: Impacts of the Indian Ocean on the  
781 ENSO cycle, *Geophys. Res. Lett.*, 29(8), 1204, 2002.

782 Yu, J. and Kao, H.: Decadal changes of ENSO persistence barrier in SST and ocean heat content indices :  
783 1958 – 2001, *J. Geophys. Res.*, 112(D13), 1–10, doi:10.1029/2006JD007654, 2007.

784 Yu, Y., Notaro, M., Liu, Z., Wang, F., Alkolibi, F., Fadda, E. and Bakhrjy, F.: Climatic controls on the  
785 interannual to decadal variability in Saudi Arabian dust activity: Toward the development of a  
786 seasonal dust prediction model, *J. Geophys. Res. Atmos.*, 120(5), 1739–1758,  
787 doi:10.1002/jgrc.20224, 2015.

788 Yuan, Y. and Yang, S.: Impacts of Different Types of El Niño on the East Asian Climate: Focus on  
789 ENSO Cycles, *J. Clim.*, 25(21), 7702–7722, 2012.

790